

Thermodynamic Characterization of the Unfolding of the Prion Protein

Roumita Moulick and Jayant B. Udgaonkar*

National Centre for Biological Sciences, Tata Institute of Fundamental Research, Bangalore, India

ABSTRACT The prion protein appears to be unusually susceptible to conformational change, and unlike nearly all other proteins, it can easily be made to convert to alternative misfolded conformations. To understand the basis of this structural plasticity, a detailed thermodynamic characterization of two variants of the mouse prion protein (moPrP), the full-length moPrP (23–231) and the structured C-terminal domain, moPrP (121–231), has been carried out. All thermodynamic parameters governing unfolding, including the changes in enthalpy, entropy, free energy, and heat capacity, were found to be identical for the two protein variants. The N-terminal domain remains unstructured and does not interact with the C-terminal domain in the full-length protein at pH 4. Moreover, the enthalpy and entropy of unfolding of moPrP (121–231) are similar in magnitude to values reported for other proteins of similar size. However, the protein has an unusually high native-state heat capacity, and consequently, the change in heat capacity upon unfolding is much lower than that expected for a protein of similar size. It appears, therefore, that the native state of the prion protein undergoes substantial fluctuations in enthalpy and hence, in structure.

INTRODUCTION

The prion protein appears to possess unusual structural plasticity. Unlike the case with virtually any other protein, an interaction of the native cellular prion protein (PrP^C) with its infectious, misfolded, conformational isoform, the scrapie prion protein (PrP^{Sc}) results in the autocatalytic conversion of PrP^C to PrP^{Sc} (1). This process termed the prion phenomenon, has been implicated in fatal neurodegenerative diseases (2), characterized by motor disfunctioning and cerebral amyloidosis (3). It has been observed that when PrP^C from one species interacts with PrP^{Sc} from other species, a multitude of conformationally different PrP^{Sc} strains form (4,5). The easy convertibility of PrP^C is indicative of a conformationally flexible native form that may result in infinite prionability (6). The conformational flexibility of the native form is reported to be critical in prion conversion (7). It seems possible that structural fluctuations in PrP^C might drive the formation of a sparsely populated nonnative conformation capable of forming misfolded oligomers, thereby initiating the conversion of monomer to the misfolded conformation.

Three-dimensional NMR-derived structures of the recombinant mouse (8), human (9), and Syrian hamster (10) prion proteins have revealed that the native prion protein consists of a disordered N-terminal domain (NTD), and a structured C-terminal domain (CTD) comprised of three α -helices and two short β -strands. A disulphide bond between C179 in the second helix and C214 in the third helix is critical for maintaining the integrity of the protein (11). The unusual structural flexibility of the prion protein manifests itself in several ways. It results in very few amide hydrogen sites in the CTD of monomeric, recombinant human prion protein (huPrP) and full-length mouse prion

protein (moPrP (23–231)) being protected against hydrogen exchange with the solvent (12,13), compared to the number observed for other proteins of comparable size. It is apparent in the ability of huPrP to undergo domain swapping, where a dimer is formed by the swapping of the helix 3 region along with rearrangement of the disulphide bond (14). It is further apparent in the ability of the monomeric α -helical protein to also exist in an alternate, toxic, α -helical conformation (15). Unfolded prion protein, too, has been shown to form several alternative misfolded monomeric structures (16). Such conformational flexibility in both the folded and unfolded prion proteins may result in conformers that act as precursors for various types of PrP^{Sc} forms. When conformational flexibility in the folded monomeric protein was constrained artificially by introducing an additional disulphide linkage, oligomerization was found to be restrained (17). Not surprisingly, then, the monomeric protein can be made to convert into different types of aggregated forms under different experimental conditions (17–20).

Studies involving molecular dynamics simulations have attempted to elucidate qualitatively the dynamic nature of the native prion protein (21,22). These studies report high fluctuations in the loop region after β 2, in the segment connecting helices 2 and 3, and in the N-terminus of helix 1. Nevertheless, a quantitative understanding of native-state flexibility and dynamic behavior of the native prion protein has not yet been achieved. An important step in understanding such flexibility of structure quantitatively is to understand the stability of the protein in terms of thermodynamic parameters whose magnitudes are determined by structural features such as the nature and extent of the packing interactions present in the native state, the hydration of individual residues, and protein size. These thermodynamic parameters are expected to have low magnitudes for an apparently flexible protein such as the CTD of the prion protein (23).

Submitted May 29, 2013, and accepted for publication November 27, 2013.

*Correspondence: jayant@ncbs.res.in

Editor: Doug Barrick.

© 2014 by the Biophysical Society
0006-3495/14/01/0410/11 \$2.00

<http://dx.doi.org/10.1016/j.bpj.2013.11.4491>



Several aspects of prion protein stability have, however, been studied well. Chemical denaturation studies on the CTD of moPrP (moPrP (121–231)) have reported no significant difference between the stabilities of disease-associated mutant variants and that of the wild-type protein (24). Thermal denaturation studies on the CTD of huPrP (90–231) yielded similar results (25). Recent NMR-monitored studies of urea-induced unfolding at pH 7 have reported the CTD of the bovine protein to be the most stable, followed by those of the rabbit, mouse, and Syrian hamster proteins (26,27). Interestingly, these studies showed differential stabilities of different structured parts of the prion protein to urea denaturation, with the β 2 strand being the most unstable, suggesting that the unfolding process involves many microscopic intermediates. Guanidine-hydrochloride-induced unfolding of huPrP has been reported to have two-state transitions between pH 5 and pH 7, but a monomeric, β -sheet-rich unfolding intermediate may get populated below pH 5 at higher ionic strength (28). Although this study also reported that the NTD has no effect on the stability of the CTD, more recent pressure-induced denaturation studies of the moPrP have reported that stability decreases and the propensity to aggregate increases in N-terminal-deletion mutant variants (29). Hence, the role of the NTD in determining prion protein stability requires further study. It is particularly important to understand the factors governing the stability and dynamics of the prion protein, because it is known that thermodynamic stabilization of the CTD of the PrP inhibits prion infection *in vivo* (30).

In this work, two separate studies of the thermodynamics of prion protein unfolding have been carried out at pH 4, with both the recombinant full length moPrP (23–231) and its structured CTD, moPrP (121–231). An experimental condition has been found where unfolding of the native prion protein is a two state process that is essential for determination of thermodynamic parameters. A combined analysis of circular-dichroism (CD)-monitored isothermal denaturant-induced unfolding transitions and thermally induced unfolding transitions in the presence of different denaturant concentrations, along with calorimetric studies, has been carried out to determine the thermodynamic properties. The two protein variants are shown to be remarkably similar in stability and thermodynamic properties. A comparison of enthalpy, entropy and heat capacity changes with those of other globular proteins of similar size indicate a conformationally flexible and malleable native state.

EXPERIMENTAL PROCEDURES

A detailed description of materials and methods used in this study are given in the [Supporting Material](#). Briefly, isothermal urea-induced unfolding of moPrP (23–231) and moPrP (121–231) across a wide range of temperatures, and thermally induced unfolding across a wide range of denaturant concentrations, was monitored using far-ultraviolet CD spectroscopy. All data were collected using a protein concentration of 10 μ M. Each transition was analyzed to obtain the stability, $\Delta G'$, at a specific temperature and urea

concentration, as described in the [Supporting Material](#). Stability plots of $\Delta G'$ versus temperature in the absence and presence of denaturant were fit to [Eqs. S4](#) and [S16](#), respectively, in the [Supporting Material](#), yielding values of the enthalpy, $\Delta H'$, entropy, $\Delta S'$, heat capacity, $\Delta C'_p$, and midpoint of thermal denaturation temperature, T'_g , at different denaturant concentrations. Differential scanning calorimetric measurements of the two prion variants were made in the absence of denaturant to confirm thermal unfolding to be a two-state process.

Accessible surface area calculations of six proteins were made using the program PSA, and the enthalpy and entropy of hydration and internal interactions were calculated.

RESULTS

Effect of temperature on the stability of the prion protein

Isothermal urea-induced unfolding studies of moPrP (23–231) and moPrP (121–231) were performed at temperatures ranging from 276 K to 313 K. Thermally induced unfolding studies were done at concentrations of urea ranging from 0 to 3 M. In both types of studies, unfolding was monitored by far-ultraviolet CD at 222 nm. Thermally induced unfolding of native protein was also monitored by differential scanning calorimetry.

[Fig. 1, a](#) and [b](#), shows representative urea-induced equilibrium unfolding transitions of moPrP (23–231) and moPrP (121–231), respectively, at three different temperatures: 276 K, 298 K, and 313 K. The unfolding transitions show that the stabilities of the two proteins decrease with an increase in temperature. [Fig. 1, c](#) and [d](#), show thermally induced equilibrium unfolding transitions of moPrP (23–231) and moPrP (121–231), respectively. The changes in enthalpy associated with the unfolding transition obtained from van't Hoff plots of $\ln K_{app}$ versus $1/T$ (see [Eq. S21](#); [Fig. 1, c](#) and [d, insets](#)) are 55 kcal mole⁻¹ and 49 kcal mole⁻¹ at T_g values of 336.8 K and 338.0 K for moPrP (23–231) and moPrP (121–231), respectively. All equilibrium unfolding transitions, urea-induced or thermally induced, were found to be completely reversible. They were also found to be independent of protein concentration in the range 5–20 μ M ([Fig. S1](#)). All subsequent optically monitored equilibrium unfolding curves were determined using a protein concentration of 10 μ M.

[Fig. 1, e](#) and [f](#), shows the temperature dependences of the partial specific heat capacities of the two proteins. Two-state fits to the thermal scans gave values for ΔH_g (ΔH_{cal}) of 53.6 ± 2.9 kcal mole⁻¹ and 51.2 ± 3.0 kcal mole⁻¹ at T_g values of 337.0 ± 0.1 K and 337 ± 0.9 K for moPrP (23–231) and moPrP (121–231), respectively. The calorimetric van't Hoff values for ΔH_g (ΔH_{vH}) are 54.1 ± 2.2 kcal mole⁻¹ and 51.8 ± 1.3 kcal mole⁻¹ for moPrP (23–231) and moPrP (121–231), respectively. These values for ΔH_g for the two proteins from calorimetry agree well with the values obtained for the corresponding proteins from van't Hoff plots of the CD-determined thermally induced unfolding transitions. This agreement confirms the two-state nature of the thermal

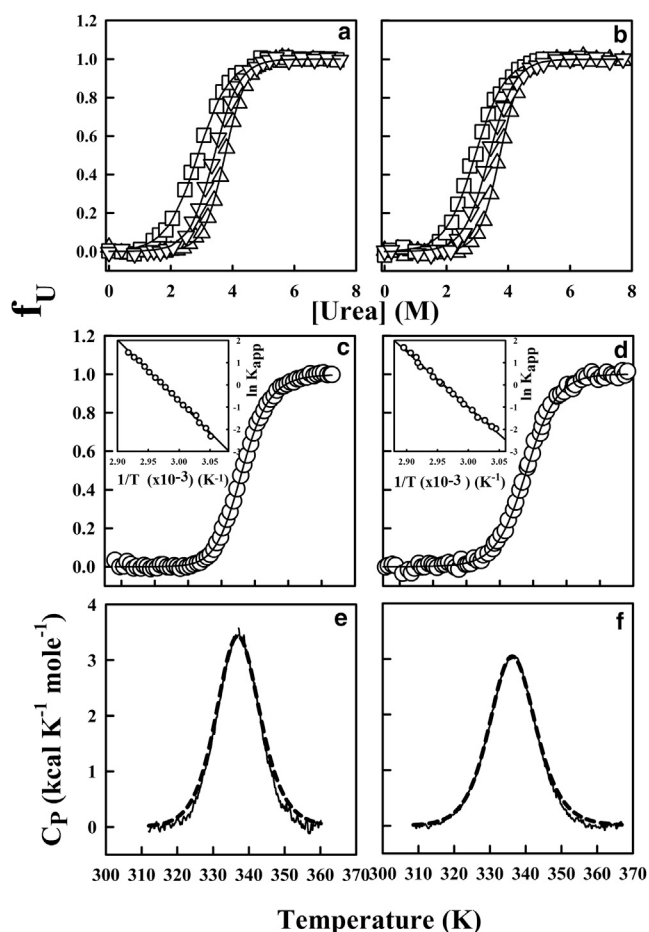


FIGURE 1 Determination of stability at pH 4 by isothermal urea-induced and thermally induced equilibrium unfolding of mouse prion protein. (a and b) Urea-induced unfolding transitions monitored by a change in mean residue ellipticity at 222 nm are shown for moPrP (23–231) (a) and moPrP (121–231) (b). The fraction of protein in the unfolded form, f_U , determined by using Eq. S19, is plotted against the concentration of urea at three different temperatures, 276 K (triangles), 298 K (inverted triangles), and 313 K (squares). The solid lines through the data are nonlinear least-squares fits of the data to Eq. S20 and yield values for ΔG , m_G , and C_m as reported in Table S1. (c and d) Thermally induced unfolding transitions in the absence of urea (circles) are shown for moPrP (23–231) (c) and for moPrP (121–231) (d). The fraction of protein in the unfolded form, f_U , is plotted against temperature. The solid lines through the data are nonlinear least-squares fits of the data to Eq. S24. (Insets) Linear least-squares fits through van't Hoff plots ($\ln K_{app}$ versus $1/T$) obtained from thermal denaturation curves are shown. (e and f) Baseline-subtracted differential scanning calorimetry scans for moPrP (23–231) (e) and moPrP (121–231) (f) with two-state fits through the data shown as black dashed lines.

equilibrium unfolding transitions of both moPrP (23–231) and moPrP (121–231).

The two-state analyses of the urea-induced unfolding transitions of moPrP (23–231) and moPrP (121–231) yielded values for ΔG , m_G , and C_m (see Fig. 2). Fig. 2a shows a stability curve of the dependence of ΔG on temperature, obtained from urea-induced unfolding transitions of moPrP (23–231) and moPrP (121–231) in the temperature range 276–313 K, and from thermally induced unfolding

transitions at temperatures >313 K. Individual fits of the ΔG data for each of the two proteins to Eq. S4 yielded thermodynamic parameters that are indistinguishable from a fit of the combined ΔG data for the two proteins. The values not only of ΔG but also of m_G and C_m are similar within experimental error for both proteins. Fig. 2, b and c, shows the temperature dependences of m_G and C_m for the two proteins. m_G is seen to have a weak dependence on temperature. Table S1 shows that the values of ΔG , m_G , and C_m are identical for both proteins at all temperatures at which these parameters were determined.

Fig. 3 shows the mean residue ellipticity values at different temperatures and urea concentrations obtained from the urea-induced unfolding transitions and the thermally induced unfolding transitions of both proteins. It is observed that as the denaturant concentration is increased, T'_g and the thermal stability decrease, as expected. It is also observed that the mean residue ellipticity at 222 nm of completely unfolded protein in 5 M urea decreases linearly with an increase in temperature. At very high temperature, it appears that the values of the mean residue ellipticities at 222 nm at different urea concentrations converge, within experimental error, to a common value of -4000 degrees $\text{cm}^2 \text{dmole}^{-1}$. This value is higher than the value expected (-2600 degrees $\text{cm}^2 \text{dmole}^{-1}$) for a random coil conformation of a polypeptide chain (31), and indicates that the unfolded state has $\sim 10\%$ of the secondary structure present in the native protein. Fig. S2 shows that the mean residue ellipticity at 222 nm of thermally unfolded protein at 360 K (where the protein appears unfolded even in the absence of urea) has a linear dependence on urea concentration, and no cooperative transition is seen. The data in Fig. 3 and Fig. S2 indicate that the mean residue ellipticity at 222 nm of unfolded protein has a linear dependence on urea concentration as well as on temperature. It should be noted that the slopes of the unfolded protein baselines, both of urea-induced unfolding curves and of thermally induced unfolding transitions, are independent of protein concentration in the range 5–20 μM (Fig. S1). The absorbance of protein samples that had been subject to either urea-induced or thermally induced unfolding (Fig. 3) was zero at and above 320 nm (data not shown), confirming that the protein does not oligomerize during unfolding.

Stability curves

A combined analysis of the isothermal urea-induced unfolding transitions obtained at temperatures ranging from 276 K to 313 K, and of the thermally induced unfolding transitions at defined urea concentrations ranging from 0 to 3 M, yield plots of free energy with respect to temperature. Fig. 4, a and b, shows such stability curves for moPrP (23–231) and moPrP (121–231) at varying urea concentrations. The $\Delta G'$ values obtained from thermally induced unfolding are

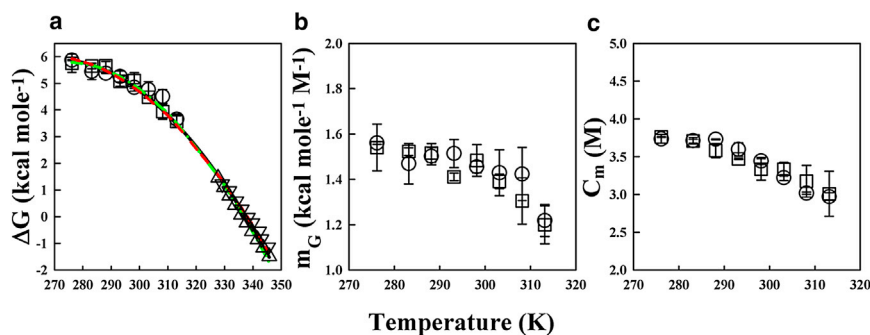


FIGURE 2 Temperature dependences of ΔG , m_G , and C_m . (a) Data from isothermal urea-induced unfolding transition (circles and squares) curves and thermally induced unfolding transition (triangles and inverted triangles) curves are shown for moPrP (23–231) and moPrP (121–231), respectively. The solid line through the combined ΔG data of moPrP (23–231) and moPrP (121–231) is a nonlinear least-squares fit to Eq. S4. The values obtained for $\Delta H'_g$, T'_g , and $\Delta C'_p$ are listed in Table 1. The green dashed and red dashed lines are fits of the ΔG data of moPrP (23–231) and moPrP (121–231), respectively, to Eq. S4, and both individual fits are virtually identical with the combined fit. (b and c) m_G values for moPrP (23–231) and moPrP (121–231) (b) and C_m values for moPrP (23–231) and moPrP (121–231) (c) as obtained from a two-state analysis of the isothermal urea-induced unfolding transitions. In both b and c, circles represent data for moPrP (23–231) and squares represent data for moPrP (121–231). The error bars represent the mean \pm SD obtained from three independent experiments. To see this figure in color, go online.

observed to be in continuity with values obtained from urea-induced unfolding. It is seen that at each urea concentration, the stability curve of moPrP (23–231) overlays completely on the stability curve of moPrP (121–231). Hence, the data for the two proteins at any denaturant concentration were fit together to Eq. S16, just as the stability data for the two proteins in the absence of urea were fit together to Eq. S4. The values obtained from such combined fits for $\Delta H'_g$, T'_g and $\Delta C'_p$ are listed in Table 1. As expected, the values of T'_g agree well with the values obtained by directly fitting the thermally induced unfolding transitions to Eq. S24. It should be noted that although in the temperature range studied each stability curve does not show a decrease in $\Delta G'$ values at lower temperatures, sufficient curvature is observed in each stability curve for reliable values of $\Delta C'_p$ to be obtained (see below). The value of $\Delta C'_p$ for moPrP (121–231) from calorimetric studies is $780 \pm 20 \text{ cal K}^{-1} \text{ mole}^{-1}$, similar to the value of $790 \pm 40 \text{ cal K}^{-1} \text{ mole}^{-1}$

obtained from the combined stability plots. The value of $\Delta C'_p$ for moPrP (23–231) could not be determined because of the high slopes of the native and unfolded protein baselines that made them intersect in the middle of the thermal transition.

Evaluation of the actual enthalpy change of unfolding

The data in Figs. 3 and 4 and in Table 1 show that the temperature of heat denaturation, T'_g , can be varied over a 30 K range by varying urea concentration. Analysis of the data in Fig. 4 yields the value of $\Delta H'_g$ at each temperature, T'_g . The value of $\Delta H'_g$ at T'_g includes the contribution $\Delta H'_i(T'_g) \cdot [D]$, where $\Delta H'_i(T'_g)$ is the preferential enthalpy of interaction of urea with the unfolded state relative to that with the folded state. Hence, the value of $\Delta H'_g$ has to be corrected to obtain the true $\Delta H'_g$ ($\Delta H'_{g \text{ cor}}$) at T'_g by subtracting out

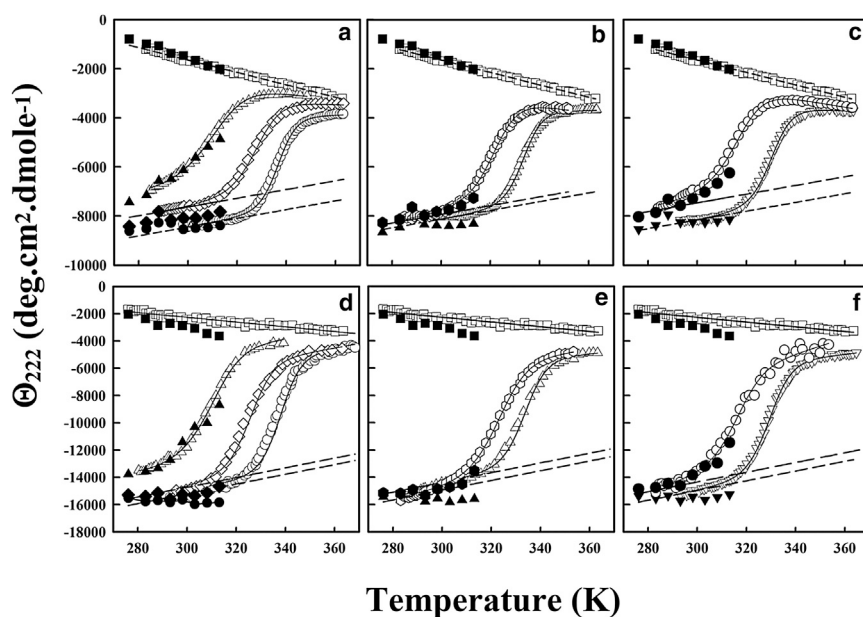


FIGURE 3 Dependences of the mean residue ellipticity at 222 nm on temperature and urea concentration. (a–c) Unfolding transitions for moPrP (23–231). (d–f) Unfolding transitions for moPrP (121–231). Open and closed symbols were obtained from thermally and urea-induced unfolding transitions, respectively. The straight dashed lines represent the globally unfolded (top lines) and folded protein (bottom lines) baselines. The former is a linear, least-squares fit to data obtained in the presence of 5 M urea, whereas the latter varies for 0 to 3 M urea. (a and d) Data for 0 M (circles), 1.5 M (diamonds), 3 M (triangles), and 5 M urea (squares). (b and e) Data for 0.5 M (triangles), 2 M (hexagons); and 5 M urea (squares). (c and f) Data for 1 M (inverted triangles), 2.5 M (circles), and 5 M urea (squares).

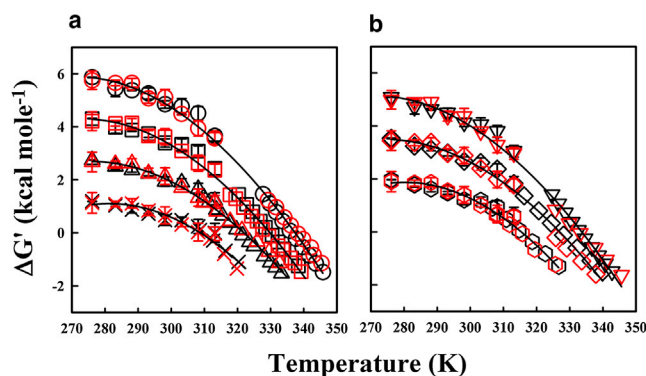


FIGURE 4 Stability curves of mouse prion protein at pH 4 in the presence of different concentrations of urea. $\Delta G'$ values at each temperature and each urea concentration from 0 to 3 M were determined from the data shown in Fig. 3. (a and b) Stability curves for moPrP (23–231) and moPrP (121–231) at different concentrations of urea: 0 M (circles), 1 M (squares), 2 M (triangles), and 3 M (x symbols) (a); and 0.5 M (inverted triangles), 1.5 M (diamonds), and 2.5 M (hexagons) (b). The black and red symbols represent data for moPrP (23–231) and moPrP (121–231), respectively. The symbols in the temperature range 276–313 K refer to data from isothermal urea-induced unfolding transitions, and symbols at other temperatures refer to data from thermal unfolding transitions. For different concentrations of urea, the $\Delta G'$ values in the temperature range 276–313 K were obtained from isothermal unfolding transitions determined at these temperatures by linear extrapolation of ΔG using Eq. S5B. Each stability curve was analyzed using a nonlinear least-squares fit to the combined $\Delta G'$ data for moPrP (23–231) and moPrP (121–231), using Eq. S16 and the values for $\Delta H'_g$, T'_g and $\Delta C'_p$ were determined for each urea concentration listed in Table 1. Nonlinear least-squares fits of the individual stability plots of moPrP (23–231) and moPrP (121–231) to Eq. S16 yielded similar values for the parameters and hence have not been shown here.

the $\Delta H'_i(T'_g)[D]$. The dependence of ΔH_i on temperature, $\Delta H'_i$, is known from the data in Fig. S4 and hence the value at T'_g ($\Delta H'_i(T'_g)$) can be determined. Fig. 5 a shows the dependence of $\Delta H'_{g \text{ cor}}$ on T'_g . The slope of this dependence gives a value of $\Delta C'_p$. The value of $\Delta C'_p$ is very similar to the value for $\Delta C'_p$ obtained from the stability curves (Fig. 4), confirming the robustness of the values obtained from the analysis of the stability curves (see above). The dependence of $\Delta C'_p$ on urea concentration is shown in Fig. 5 b. $\Delta C'_p$ is negligibly affected by urea with a dependence, $\Delta C'_{pi}$, of $24 \text{ cal K}^{-1} \text{ mole}^{-1} \text{ M}^{-1}$.

TABLE 1 Thermodynamic parameters governing the thermal denaturation of the mouse prion protein at pH 4

Urea (M)	T'_g (K)	$\Delta H'_g$ (kcal mole ⁻¹)	$\Delta S'_g$ (cal mole ⁻¹ K ⁻¹)	T'_h (K)	T'_s (K)	$\Delta G'_s$ (kcal mole ⁻¹)	$\Delta C'_p$ (cal mole ⁻¹ K ⁻¹)
0	337.4	58	172	263.9	271.3	5.9	790
0.5	333.7	53	159	264.4	271.1	5.1	765
1	329.8	49	148	268.0	273.4	4.3	788
1.5	327.0	42	129	269.5	274.3	3.5	732
2	321.9	37	114	272.1	275.7	2.7	734
2.5	315.4	33	104	278.0	280.1	1.9	876
3	308.7	24	79	280.0	281.2	1.1	846

$\Delta H'_g$ and $\Delta S'_g$ are values at temperature T'_g . $\Delta H'_g$, $\Delta S'_g$ and $\Delta C'_p$ are values obtained from nonlinear least-squares fits to the combined stability curves shown in Fig. 4. T'_h and T'_s are determined using Eqs. S25 and S26, respectively. $\Delta G'_s$ is determined using Eq. S27. Errors in the thermodynamic parameters were between 5% and 10%.

Evaluation of the native-state heat capacity

Differential scanning calorimetry was used to measure the heat capacity as a function of temperature of different concentrations of moPrP (121–231) in the range 10–30 μM . Fig. 6 a shows two representative differential calorimetric scans of moPrP (121–231) at protein concentrations of 10 and 30 μM . Fig. 6 b shows the heat capacity, C_p , at 298 K as a function of the mass of protein. This slope was used with Eq. S30 to calculate the absolute heat capacity of the native state (32) using a partial volume of 0.730 mL g^{-1} (33), and the calculations yielded a value for the native-state heat capacity of $0.590 \text{ cal K}^{-1} \text{ g}^{-1}$.

Urea-induced unfolding of moPrP at pH 7 and pH 4 in the presence of salt

The overlapping urea-induced equilibrium unfolding transitions of moPrP (23–231) and moPrP (121–231) at pH 4 indicates that the disordered NTD does not interact with the structured CTD at this pH, and hence does not contribute to the stability or to any other thermodynamic property. At pH 7, however, in good agreement with earlier studies (24), the urea-induced equilibrium unfolding transitions of the two proteins are not coincident and show a difference in stability (Fig. S6 a).

Previous studies had indicated that urea-induced unfolding at pH 4 in the presence of NaCl proceeds through an intermediate that forms oligomers (34,35). Fig. S6 b shows the urea-induced unfolding transition of moPrP (23–231) at pH 4 in the presence of 100 mM sodium chloride. The transition is broad and cannot be fit to a two-state model. Similar studies with moPrP (121–231) also yield similar results (data not shown). A size-exclusion profile of protein equilibrated in a concentration of urea near the midpoint of the transition indicates the presence of oligomeric forms that elute out in the void volume of the column (Fig. S6 b, inset, red). However, in the absence of salt, urea-induced unfolding is a two-state process, as shown in Fig. 1 a and Fig. S6 b (inset, dashed black line), and there is no evidence for any oligomeric intermediate state. It is for this reason that all urea-induced unfolding studies described in this report were carried out in the absence of added salt.

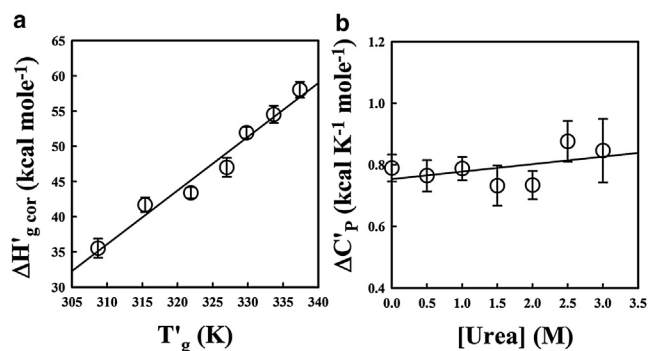


FIGURE 5 $\Delta C'_p$ of unfolding of the mouse prion protein at pH 4. (a) Dependence of $\Delta H'_{g, \text{cor}}$ on T'_g . The value of $\Delta H'_{g, \text{cor}}$ determined at each T'_g , at different urea concentrations in the range 0–3 M is corrected for the enthalpy of interaction of the denaturant using Eq. S17 and plotted against T'_g . The slope of the linear least-squares fit through the data represents an apparent $\Delta C'_p$ of $763 \pm 61 \text{ cal K}^{-1} \text{ mole}^{-1}$. (b) Dependence of $\Delta C'_p$ on urea concentration. The solid line through the data is a linear least-squares fit using Eq. S8. The slope and intercept are $24 \text{ cal K}^{-1} \text{ mole}^{-1} \text{ M}^{-1}$ and $754 \pm 35 \text{ cal K}^{-1} \text{ mole}^{-1}$, respectively. Error bars represent the standard errors determined from nonlinear least-squares analysis of the stability curves in Fig. 4 to Eq. S16.

DISCUSSION

In this study, the thermodynamics of unfolding of moPrP was studied at pH 4. Several *in vitro* studies have reported that PrP^C has a higher propensity to convert into misfolded forms at low pH and in the presence of high salt concentration (34–36). *In vivo* studies have also indicated that the conversion of PrP^C into PrP^{Sc} may take place in endosomal compartments of cells where the cellular environment is acidic (37,38). Hence, it was important to understand native-state interactions, packing of residues, and stability at acidic pH. Moreover, it was not possible to carry out a detailed thermodynamic characterization at pH 7, because thermally induced unfolding of moPrP at pH 7 is irreversible and leads to precipitation of the protein, unlike that of huPrP (90–231)

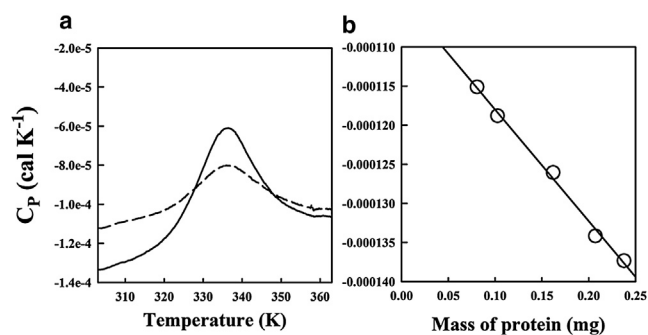


FIGURE 6 Measurement of absolute native-state heat capacity of moPrP (121–231). (a) Representative calorimetric scans obtained at protein concentrations of $10 \mu\text{M}$ (dashed line) and $30 \mu\text{M}$ (solid line). (b) Plot of heat capacity, C_p , at 298 K versus the mass of protein in the calorimetric cell. The linear least-squares fit to the data represent the dependence of heat capacity on the mass of the protein and yield a slope of $0.140 \text{ mcal K}^{-1} \text{ mg}^{-1}$.

(25). It was also important for a full thermodynamic study that unfolding be a two-state reaction, and hence, all experiments were done in the absence of added salt because it is known (Fig. S6) that the protein forms an oligomeric intermediate at higher ionic strength. The data in Fig. 1 confirm the two-state nature of the unfolding reaction under the experimental conditions utilized in this study.

Moreover, in this study, the thermodynamics of unfolding of full-length moPrP (23–231) has been compared to that of the CTD moPrP (121–231), to evaluate the contribution of the NTD to the stability of moPrP. The disordered NTD can form partial structure in its octapeptide repeat region under some conditions (39), can interact with a wide range of molecules such as lipids, RNA, and heparin sulfate glycosaminoglycans, can modulate prion protein aggregation (29,40–42), and appears to be important for prion protein function. Hence, it was important to understand the role, if any, of the NTD in modulating prion protein stability.

The presence of the NTD does not affect stability at pH 4 but does at pH 7

It is known that even a single amino acid residue N-terminal extension to the sequence of a protein may affect its stability (43–46). It is therefore remarkable that the 99 residue disordered NTD of moPrP does not affect the stability of the protein at pH 4 (Table S1). On the other hand, the NTD does affect stability at pH 7. There are two possible explanations. One possibility is that deprotonation of one or more residues in either the CTD or the NTD at pH 7 allows the NTD to interact with the CTD, presumably through electrostatic interactions, which consequently modulates stability at pH 7. The other possibility is that the NTD in moPrP (23–231) is partially structured at pH 7 but not at pH 4, as has been reported (39). Such structure might be expected to enhance the stability of moPrP (23–231) at pH 7, but only a marginal increase in stability is observed from our studies (Fig. 1 and Fig. S6). On the other hand, the increase in the stability of moPrP (121–231) upon increasing pH from 4 to 7 is significantly higher (Figs. 1 a and S6 a), in agreement with previous studies on huPrP (28). Hence, at pH 7, moPrP (121–231) is more stable than moPrP (23–231) by 1 kcal mole^{-1} (Fig. S6 a). Thus, it is unlikely that any significant stabilizing structure is present in the NTD of moPrP (23–231) at pH 7.

Not only are the free energies of unfolding, ΔG , of moPrP (23–231) and moPrP (121–231) identical at each of the temperatures at which the stabilities are measured, but so are the dependences of these values on urea concentration, given by m_G . m_G , which is a measure of the surface area exposed upon unfolding, scales linearly with protein size (47), and the value of m_G for the structured moPrP (121–231) is as expected for a protein of its size. The observation that the values of m_G for moPrP (23–231) and moPrP (121–231) are identical at each of the temperatures at which they were determined at pH 4, supports the conclusion that native

moPrP (23–231) does not possess any structure in its NTD at pH 4, because unfolding of that structure would have led to an increase in exposed surface area upon the unfolding of moPrP (23–231) relative to the unfolding of moPrP (121–231). The weak dependence of m_G (Figs. 2 *b* and S4 *c*) on temperature is explained by the very small magnitude of ΔC_{P_i} (24 cal K⁻¹ mole⁻¹ M⁻¹).

In addition to the magnitudes of ΔG and m_G (or ΔG_i) being identical for moPrP (23–231) and moPrP (121–231) at pH 4 (see Table S1), the stability curves from the CD-monitored unfolding transitions (Fig. 3) yield similar values of ΔH_g , T_g , and ΔC_p for the two proteins. Indeed all thermodynamic parameters are identical for moPrP (23–231) and moPrP (121–231) across the range of urea concentrations as well as the temperatures studied (see Table 1).

The thermodynamic parameters listed in Table 1 and Fig. S5 indicate that in 3.57 M urea and at a temperature of 282.7 K, $T'_s = T'_h$ and $\Delta G' = \Delta H' = \Delta S' = 0$. Under this unique unfolding condition, the folded and unfolded states, present in equal amounts, will not differ in either enthalpy or entropy. In future studies, it will be important to determine how the folded and unfolded states differ in structural terms, and what the nature of the folding and unfolding transitions is, under this unique unfolding condition.

Enthalpy and entropy of unfolding

One goal of this study was to determine whether the thermodynamic parameters governing the unfolding of moPrP have unusual values compared to the values obtained for other globular proteins. It is possible to dissect the enthalpy and entropy changes into two components, with one component (ΔH^{hyd} , ΔS^{hyd}) originating from the change in the hydration of polar and nonpolar moieties upon unfolding, and the other component (ΔH^{int} , ΔS^{int}) originating from the changes in the internal interactions and conformational entropy upon unfolding (48,49). Using model compound data and calculating the changes in nonpolar and polar surface area upon unfolding (see Methods in the Supporting Material), ΔH^{hyd} and ΔS^{hyd} for moPrP (121–231) were determined, from which ΔH^{int} and ΔS^{int} were then determined (Table S2). Here, the values of ΔH^{exp} and ΔS^{exp} at different temperatures, for the proteins to which moPrP is being compared, were taken from Robertson and Murphy (50).

ΔH^{hyd} favors unfolding, but ΔS^{hyd} favors folding because of the increase in the disorder of the water molecules that are released from hydrogen bonding upon folding (Fig. S4). Hence, as reported previously for other proteins (48,49,51), overall, hydration favors unfolding, more so at lower temperatures, where it would be responsible for cold denaturation. But it should be noted that there might be an error in the estimation of the contribution of peptide solvation to ΔH^{hyd} when monoamide solvation data are used, because electrostatic interactions between dipoles of neighboring peptide groups in the peptide backbone (the

peptide desolvation penalty) are not taken into account (52,53); indeed, the burial of polar groups has been reported to contribute substantially to protein stability (54). Nevertheless, it seems still possible to compare ΔH^{hyd} , ΔS^{hyd} , ΔH^{int} , and ΔS^{int} for moPrP (121–231) to proteins of similar size, for the purpose of determining whether moPrP is unusual in its thermodynamic properties.

ΔH^{int} represents the change in van der Waals interactions and interactions between polar groups during unfolding of the protein in vacuum and is known to decrease slightly with temperature due to thermal expansion of the native state (55), N, as observed in Fig. S7 *b*. ΔS^{int} favors unfolding, because that leads to an increase in the disorder of the polypeptide and the side chains and destabilizes the N state more at higher temperature (Fig. S7 *d*). Hence, as reported for the other proteins (48,49,51) overall, internal interactions (hydrogen bonding and van der Waals interactions) are seen to be responsible for stabilizing the N state because of their strong enthalpic contributions. The observation that these thermodynamic parameters for moPrP (121–231) are similar in value to those for other globular proteins (Fig. S7) suggests in particular that the extent of packing interactions in the structured part of moPrP is not much different from that in other globular proteins. However, it could also be the case that these parameters do not depend on packing density, and, in fact, it has been suggested that the enthalpy of unfolding (per amino acid residue) is independent of packing density for globular proteins (56).

A comparison of the temperature dependences of ΔH_{npl}^{hyd} and ΔS_{npl}^{hyd} for moPrP (121–231) to the values calculated for the other reference proteins (Fig. S8) shows that the values of either parameter are nearly identical for moPrP and all the other proteins at all temperatures, and that the negative values of ΔH_{npl}^{hyd} and ΔS_{npl}^{hyd} decrease in magnitude to become zero at 366 K and 397 K, respectively (Fig. S8, *a* and *c*), as reported previously (48,49). The significance of these temperatures still needs to be understood. For moPrP (121–231) and the other proteins, ΔH_{pol}^{hyd} favors unfolding, whereas ΔS_{pol}^{hyd} favors folding. Overall, the hydration of polar parts favors unfolding, much more than the hydration of nonpolar parts favors folding. Although both ΔS_{pol}^{hyd} and ΔS_{npl}^{hyd} favor folding, the contribution of polar hydration to the overall entropy of hydration is more than that of nonpolar hydration. The observation that the hydration of nonpolar surface as well as internal interactions (van der Waals and hydrogen bonding) both stabilize moPrP to a substantial extent, is in agreement with a recent study of the relative contribution of hydrophobic interactions to protein stability (57).

Change in heat capacity

Protein unfolding reactions are characterized by a large positive increase in heat capacity (ΔC_p), which is thought to have a contribution not only from the hydrophobic effect

(arising from the change in hydration of nonpolar surface upon unfolding) but also from changes in electrostatic interactions, hydrogen bonding, conformational entropy, and intramolecular vibrational modes upon unfolding (58,59). From a study of 49 different proteins (50), it is known that ΔC_P is accurately proportional to N_R , the number of residues in a protein, and that the value of $\Delta C_P/N_R$ is $13.9 \pm 0.5 \text{ cal K}^{-1} \text{ mole}^{-1}$. The value of $\Delta C_P/N_R$ for moPrP (121–231) is, however, only $7.2 \text{ cal K}^{-1} \text{ mole}^{-1}$, about half the expected value.

Studies of the dependence of ΔC_P on the change in accessible surface area upon unfolding (47) have shown that a change in the hydration of nonpolar surface area is the predominant positive contributor to the ΔC_P of unfolding, whereas the change in polar surface area makes a smaller, negative contribution to the ΔC_P of unfolding. For moPrP (121–231), the changes in polar, nonpolar, and total accessible surface areas are 4989 \AA^2 , 6069 \AA^2 , and $11,058 \text{ \AA}^2$, respectively, which are the values expected for a protein of its size (50). The observation that the increase in polar surface area upon unfolding, which can be attributed to helix unfolding, is as expected and not excessively large, indicates that the observed value of $\Delta C_P/N_R$ is not low because of the decrease in heat capacity associated with helix unfolding, for which $\Delta C_P/N_R = -7.5 \text{ cal K}^{-1} \text{ mole}^{-1}$ (60).

Fig. S9 shows the ΔC_P values for moPrP (121–231) and 40 other reference globular proteins (50), plotted against the changes in their accessible nonpolar surface area upon unfolding. It is to be noted here that the nonpolar accessible surface areas of all proteins have been corrected for the effect of disulphides (if present, as described in the Supporting Material), which increase compactness in the unfolded state, thereby reducing the unfolded-state accessible surface area (47). A major outcome of this study is the observation that the $\Delta C_P/N_R$ of unfolding for moPrP (121–231) has almost half the value predicted for a protein with a similar change in average nonpolar accessible surface area.

The simplest explanation for the low heat capacity change upon unfolding would be that the native state of moPrP (121–231) is not as well packed as the native states of other proteins (23), but this explanation is not validated by the observation that both $\Delta C_P/N_R$ and $\Delta H/N_R$ for unfolding are independent of packing density in globular proteins (56). In any case, the value of ΔH^{int} for moPrP (121–231) is as expected for a protein of its size and is comparable to that of other globular proteins (Fig. S7 b).

The second explanation could be that residual structure is present in the unfolded state. In that case, the change in accessible nonpolar surface area upon unfolding of moPrP (121–231) would be smaller, leading to a smaller value of ΔC_P . Native-state hydrogen-exchange studies with the Syrian hamster and human prion proteins have shown that ~10 amide hydrogens belonging to both nonpolar and polar residues adjacent to the disulphide bond formed by C179 and C214, are protected (superprotected) more than pre-

dicted by the global stability of the protein, which suggests that partial structure involving these residues is present either in the unfolded state in native conditions or in a high-energy intermediate (12,61). It is likely that the partial structure is present in a high-energy intermediate, which has been identified in kinetic studies (62), is responsible for the superprotection against hydrogen exchange. If, however, partial structure is also present in the unfolded state, as appears to be the case, since the mean residue ellipticity at 222 nm of the unfolded protein is ~15% of that of the native state (see Results), it appears to involve the formation of a cluster around the disulphide bond by only about 10 residues. Of the total area (~11,000 \AA^2) that would be exposed upon unfolding of moPrP (121–231) to a random coil, the nonpolar surface area exposed would be 6069 \AA^2 , and of this, only 753 \AA^2 would be contributed by the 10 residues with the superprotected amides. Thus, even if these residues were to remain as buried in the unfolded state as they are in the native state, the ΔC_P value would be lower by only ~15%. In this context, it should also be noted that the m_G value which represents the total nonpolar and polar surface area exposed upon unfolding, is what is expected for a protein of the size of moPrP (121–231). It therefore appears that any structure in the unfolded state can account for the ΔC_P value being only ~15% less than its expected value, and not 50% less, as observed.

The observations that the value of ΔC_P is essentially independent of urea concentration (Fig. 5 b) and that the mean residue ellipticity of the unfolded state changes linearly with both an increase in urea concentration and an increase in temperature (Fig. 3) suggest that the ellipticity may not arise from specific structure that can melt in a cooperative manner. The linear dependence of the mean residue ellipticity of the unfolded protein on both temperature and urea concentration has been seen for other proteins (63–66) and possibly represents gradual structural change in the unfolded state. It should also be noted that if there were interactions present in any residual structure in the unfolded state, and if they were more labile to an increase in temperature than the interactions present in the native state, then the enthalpy of the unfolded state would increase more than that of the native state with an increase in temperature, and the value of ΔC_P would in fact be higher.

The most plausible explanation for the low ΔC_P of unfolding is an unusually high level of structural fluctuations in the native state. Such fluctuations would lead to large fluctuations in the enthalpy of the native state, and hence to a higher heat capacity for the native state. The increase in ΔC_P upon unfolding for moPrP (121–231) would then be smaller than for other proteins whose native states exhibit lower levels of structural and enthalpy fluctuations. Indeed, the value of the absolute heat capacity of the native state of moPrP (121–231), $0.590 \text{ cal K}^{-1} \text{ g}^{-1}$ (Fig. 6), is much larger than values reported for other proteins, which lie in the range of $0.330\text{--}0.390 \text{ cal K}^{-1} \text{ g}^{-1}$ (67). A native state that

is fluctuating at fast timescales and sampling other conformations that are less compact and hence more solvent-accessible will result in a low heat-capacity change of unfolding averaged over these conformations, as heat capacity is additive with respect to its contributions mentioned above (67). This result is in good agreement with native-state hydrogen-deuterium exchange studies (13), where it was observed that most parts of the CTD of moPrP (23–231) exchange out rapidly, and that only 14 backbone amide hydrogen atoms are protected and that, too, for a short time. In contrast, other proteins of similar size, such as those with which the prion protein is compared in Figs. S7 and S8, have about three times the number of protected amide hydrogens, and the level of protection is substantially larger (68–72). This suggests that the fluctuations in the native state of moPrP (121–231) are unusually large compared to those in the native states of other proteins. Nevertheless, NMR studies have identified only two short-sequence segments within the CTD of moPrP, residues 167–171 and 188–193, as flexibly disordered (73).

CONCLUSION

The detailed characterization of the thermodynamics of unfolding of the moPrP, carried out in this study, has strikingly brought out its unusual structural malleability. The prion protein appears to be highly dynamic in nature as reflected in its high absolute native-state heat capacity and consequent low change in heat capacity upon unfolding. The highly dynamic nature of the prion protein would make it more amenable to a change in conformation of the type that leads to an aggregation-prone misfolded state (N*) and to aggregation. Such aggregation-prone states have been identified for other proteins too, and it appears that the ease of accessibility of N* determines whether the protein will aggregate on relevant timescales (74,75). The results presented here suggest that the prion protein can access aggregation-prone states with relative ease.

The observation that the NTD does not interact sufficiently with the CTD to affect the stability of moPrP (23–231) is surprising, because the NTD does modulate prion protein aggregation. N-terminal deletion mutants have a lower propensity to convert into aggregated forms (29) while the presence of the NTD leads to bigger aggregates as compared to those formed by only the CTD. In vivo studies have reported that mice expressing N-terminally truncated PrP develop disease more slowly and have lower prion titers than mice expressing full-length PrP (41,76). The NTD is also known to interact with A β 42 oligomers, which may be critical in pathological conditions (77). It will be important in future studies to understand how the NTD interacts with the CTD to affect prion protein aggregation, and it is likely that the unusual malleability of the CTD structure allows it to interact with the NTD in a manner that modulates prion disease pathology.

SUPPORTING MATERIAL

Thirty equations, two tables, nine figures, references (78–87) and Supporting Materials and Methods are available at [http://www.biophysj.org/biophysj/supplemental/S0006-3495\(13\)05752-4](http://www.biophysj.org/biophysj/supplemental/S0006-3495(13)05752-4).

We would like to thank Prof. R. Varadarajan for discussions, for the program PSA and for the use of the calorimeter in his laboratory, and Prof. M. K. Mathew for discussions. We would also like to thank Hemant Giri Rao for helping us with accessible surface area calculations. We thank our laboratory members for discussions. JBU is the recipient of JC Bose National Fellowship from the Government of India.

This work was funded by the Tata Institute of Fundamental Research, and by the Department of Science and Technology, Government of India.

REFERENCES

1. Prusiner, S. B. 1991. Molecular biology of prion diseases. *Science*. 252:1515–1522.
2. Horiuchi, M., and B. Caughey. 1999. Prion protein interconversions and the transmissible spongiform encephalopathies. *Structure*. 7:R231–R240.
3. Gajdusek, D. C. 1977. Unconventional viruses and the origin and disappearance of kuru. *Science*. 197:943–960.
4. Prusiner, S. B. 1998. Prions. *Proc. Natl. Acad. Sci. USA*. 95:13363–13383.
5. Bessen, R. A., D. A. Kocisko, ..., B. Caughey. 1995. Non-genetic propagation of strain-specific properties of scrapie prion protein. *Nature*. 375:698–700.
6. Soto, C. 2011. Prion hypothesis: the end of the controversy? *Trends Biochem. Sci.* 36:151–158.
7. Scheibel, T., and S. L. Lindquist. 2001. The role of conformational flexibility in prion propagation and maintenance for Sup35p. *Nat. Struct. Biol.* 8:958–962.
8. Riek, R., S. Hornemann, ..., K. Wüthrich. 1997. NMR characterization of the full-length recombinant murine prion protein, mPrP(23–231). *FEBS Lett.* 413:282–288.
9. Zahn, R., A. Liu, ..., K. Wüthrich. 2000. NMR solution structure of the human prion protein. *Proc. Natl. Acad. Sci. USA*. 97:145–150.
10. Donne, D. G., J. H. Viles, ..., H. J. Dyson. 1997. Structure of the recombinant full-length hamster prion protein PrP(29–231): the N terminus is highly flexible. *Proc. Natl. Acad. Sci. USA*. 94:13452–13457.
11. Maiti, N. R., and W. K. Surewicz. 2001. The role of disulfide bridge in the folding and stability of the recombinant human prion protein. *J. Biol. Chem.* 276:2427–2431.
12. Hosszu, L. L. P., N. J. Baxter, ..., J. Collinge. 1999. Structural mobility of the human prion protein probed by backbone hydrogen exchange. *Nat. Struct. Biol.* 6:740–743.
13. Singh, J., A. T. Sabareesan, ..., J. B. Udgaonkar. 2012. Development of the structural core and of conformational heterogeneity during the conversion of oligomers of the mouse prion protein to worm-like amyloid fibrils. *J. Mol. Biol.* 423:217–231.
14. Knaus, K. J., M. Morillas, ..., V. C. Yee. 2001. Crystal structure of the human prion protein reveals a mechanism for oligomerization. *Nat. Struct. Biol.* 8:770–774.
15. Zhou, M., G. Ottenberg, ..., C. I. Lasmézas. 2012. Highly neurotoxic monomeric α -helical prion protein. *Proc. Natl. Acad. Sci. USA*. 109:3113–3118.
16. Yu, H., X. Liu, ..., M. T. Woodside. 2012. Direct observation of multiple misfolding pathways in a single prion protein molecule. *Proc. Natl. Acad. Sci. USA*. 109:5283–5288.
17. Eghiaian, F., T. Daubenfeld, ..., H. Rezaei. 2007. Diversity in prion protein oligomerization pathways results from domain expansion as

- revealed by hydrogen/deuterium exchange and disulfide linkage. *Proc. Natl. Acad. Sci. USA.* 104:7414–7419.
18. Zhang, H., J. Stöckel, ..., F. E. Cohen. 1997. Physical studies of conformational plasticity in a recombinant prion protein. *Biochemistry.* 36:3543–3553.
 19. Makarava, N., and I. V. Baskakov. 2008. The same primary structure of the prion protein yields two distinct self-propagating states. *J. Biol. Chem.* 283:15988–15996.
 20. Jain, S., and J. B. Udgaonkar. 2010. Salt-induced modulation of the pathway of amyloid fibril formation by the mouse prion protein. *Biochemistry.* 49:7615–7624.
 21. Gsponer, J., P. Ferrara, and A. Cafisch. 2001. Flexibility of the murine prion protein and its Asp178Asn mutant investigated by molecular dynamics simulations. *J. Mol. Graph. Model.* 20:169–182.
 22. Guilbert, C., F. Ricard, and J. C. Smith. 2000. Dynamic simulation of the mouse prion protein. *Biopolymers.* 54:406–415.
 23. Wintrode, P. L., Y. V. Griko, and P. L. Privalov. 1995. Structural energetics of barstar studied by differential scanning microcalorimetry. *Protein Sci.* 4:1528–1534.
 24. Liemann, S., and R. Glockshuber. 1999. Influence of amino acid substitutions related to inherited human prion diseases on the thermodynamic stability of the cellular prion protein. *Biochemistry.* 38:3258–3267.
 25. Swietnicki, W., R. B. Petersen, ..., W. K. Surewicz. 1998. Familial mutations and the thermodynamic stability of the recombinant human prion protein. *J. Biol. Chem.* 273:31048–31052.
 26. Julien, O., S. Chatterjee, ..., B. D. Sykes. 2009. Differential stability of the bovine prion protein upon urea unfolding. *Protein Sci.* 18:2172–2182.
 27. Julien, O., S. Chatterjee, ..., N. R. Cashman. 2011. Relative and regional stabilities of the hamster, mouse, rabbit, and bovine prion proteins toward urea unfolding assessed by nuclear magnetic resonance and circular dichroism spectroscopies. *Biochemistry.* 50:7536–7545.
 28. Swietnicki, W., R. Petersen, ..., W. K. Surewicz. 1997. pH-dependent stability and conformation of the recombinant human prion protein PrP(90–231). *J. Biol. Chem.* 272:27517–27520.
 29. Cordeiro, Y., J. Kraineva, ..., J. L. Silva. 2005. The amino-terminal PrP domain is crucial to modulate prion misfolding and aggregation. *Biophys. J.* 89:2667–2676.
 30. Kong, Q., J. L. Mills, ..., W. K. Surewicz. 2013. Thermodynamic stabilization of the folded domain of prion protein inhibits prion infection in vivo. *Cell Rep.* 4:248–254.
 31. Chen, Y. H., J. T. Yang, and H. M. Martinez. 1972. Determination of the secondary structures of proteins by circular dichroism and optical rotatory dispersion. *Biochemistry.* 11:4120–4131.
 32. Kholodenko, V., and E. Freire. 1999. A simple method to measure the absolute heat capacity of proteins. *Anal. Biochem.* 270:336–338.
 33. Squire, P. G., and M. E. Himmel. 1979. Hydrodynamics and protein hydration. *Arch. Biochem. Biophys.* 196:165–177.
 34. Hornemann, S., and R. Glockshuber. 1998. A scrapie-like unfolding intermediate of the prion protein domain PrP(121–231) induced by acidic pH. *Proc. Natl. Acad. Sci. USA.* 95:6010–6014.
 35. Khan, M. Q., B. Sweeting, ..., A. Chakrabarty. 2010. Prion disease susceptibility is affected by β -structure folding propensity and local side-chain interactions in PrP. *Proc. Natl. Acad. Sci. USA.* 107:19808–19813.
 36. Bjorndahl, T. C., G. P. Zhou, ..., D. S. Wishart. 2011. Detailed biophysical characterization of the acid-induced PrP^c to PrP^B conversion process. *Biochemistry.* 50:1162–1173.
 37. Borchelt, D. R., A. Taraboulos, and S. B. Prusiner. 1992. Evidence for synthesis of scrapie prion proteins in the endocytic pathway. *J. Biol. Chem.* 267:16188–16199.
 38. Arnold, J. E., C. Tipler, ..., R. J. Mayer. 1995. The abnormal isoform of the prion protein accumulates in late-endosome-like organelles in scrapie-infected mouse brain. *J. Pathol.* 176:403–411.
 39. Zahn, R. 2003. The octapeptide repeats in mammalian prion protein constitute a pH-dependent folding and aggregation site. *J. Mol. Biol.* 334:477–488.
 40. Flechsig, E., D. Shmerling, ..., C. Weissmann. 2000. Prion protein devoid of the octapeptide repeat region restores susceptibility to scrapie in PrP knockout mice. *Neuron.* 27:399–408.
 41. Lawson, V. A., S. A. Priola, ..., B. Chesebro. 2004. Flexible N-terminal region of prion protein influences conformation of protease-resistant prion protein isoforms associated with cross-species scrapie infection in vivo and in vitro. *J. Biol. Chem.* 279:13689–13695.
 42. Moore, R. A., C. Herzog, ..., S. A. Priola. 2006. Octapeptide repeat insertions increase the rate of protease-resistant prion protein formation. *Protein Sci.* 15:609–619.
 43. Hargrove, M. S., S. Krzywda, ..., J. S. Olson. 1994. Stability of myoglobin: a model for the folding of heme proteins. *Biochemistry.* 33:11767–11775.
 44. Imoto, T., H. Yamada, ..., T. Horiuchi. 1987. Point mutation of alanine (31) to valine prohibits the folding of reduced lysozyme by sulfhydryl-disulfide interchange. *Protein Eng.* 1:333–338.
 45. Chaudhuri, T. K., K. Horii, ..., I. Kumagai. 1999. Effect of the extra N-terminal methionine residue on the stability and folding of recombinant α -lactalbumin expressed in *Escherichia coli*. *J. Mol. Biol.* 285:1179–1194.
 46. Schultz, D. A., and R. L. Baldwin. 1992. Cis proline mutants of ribonuclease A. I. Thermal stability. *Protein Sci.* 1:910–916.
 47. Myers, J. K., C. N. Pace, and J. M. Scholtz. 1995. Denaturant m values and heat capacity changes: relation to changes in accessible surface areas of protein unfolding. *Protein Sci.* 4:2138–2148.
 48. Makhatadze, G. I., and P. L. Privalov. 1993. Contribution of hydration to protein folding thermodynamics. I. The enthalpy of hydration. *J. Mol. Biol.* 232:639–659.
 49. Privalov, P. L., and G. I. Makhatadze. 1993. Contribution of hydration to protein folding thermodynamics. II. The entropy and Gibbs energy of hydration. *J. Mol. Biol.* 232:660–679.
 50. Robertson, A. D., and K. P. Murphy. 1997. Protein structure and the energetics of protein stability. *Chem. Rev.* 97:1251–1268.
 51. Makhatadze, G. I., and P. L. Privalov. 1994. Hydration effects in protein unfolding. *Biophys. Chem.* 51:291–304, discussion 304–309.
 52. Baldwin, R. L. 2007. Energetics of protein folding. *J. Mol. Biol.* 371:283–301.
 53. Baldwin, R. L. 2010. Desolvation penalty for burying hydrogen-bonded peptide groups in protein folding. *J. Phys. Chem. B.* 114:16223–16227.
 54. Pace, C. N., G. Horn, ..., J. Sevcik. 2001. Tyrosine hydrogen bonds make a large contribution to protein stability. *J. Mol. Biol.* 312:393–404.
 55. Makhatadze, G. I., and P. L. Privalov. 1995. Energetics of protein structure. *Adv. Protein Chem.* 47:307–425.
 56. Liang, J., and K. A. Dill. 2001. Are proteins well-packed? *Biophys. J.* 81:751–766.
 57. Pace, C. N., H. Fu, ..., G. R. Grimsley. 2011. Contribution of hydrophobic interactions to protein stability. *J. Mol. Biol.* 408:514–528.
 58. Sturtevant, J. M. 1977. Heat capacity and entropy changes in processes involving proteins. *Proc. Natl. Acad. Sci. USA.* 74:2236–2240.
 59. Prabhu, N. V., and K. A. Sharp. 2005. Heat capacity in proteins. *Annu. Rev. Phys. Chem.* 56:521–548.
 60. Richardson, J. M., and G. I. Makhatadze. 2004. Temperature dependence of the thermodynamics of helix-coil transition. *J. Mol. Biol.* 335:1029–1037.
 61. Nicholson, E. M., H. Mo, ..., S. Marqusee. 2002. Differences between the prion protein and its homolog Doppel: a partially structured state with implications for scrapie formation. *J. Mol. Biol.* 316:807–815.
 62. Chen, K. C., M. Xu, ..., H. Roder. 2011. Microsecond unfolding kinetics of sheep prion protein reveals an intermediate that correlates with susceptibility to classical scrapie. *Biophys. J.* 101:1221–1230.

63. Pace, N. C., and C. Tanford. 1968. Thermodynamics of the unfolding of β -lactoglobulin A in aqueous urea solutions between 5 and 55°. *Biochemistry*. 7:198–208.
64. Nojima, H., K. Hon-Nami, ..., H. Noda. 1978. Reversible thermal unfolding of thermostable cytochrome *c*-552. *J. Mol. Biol.* 122:33–42.
65. Privalov, P. L., E. I. Tiktopulo, ..., N. N. Khechinashvili. 1989. Heat capacity and conformation of proteins in the denatured state. *J. Mol. Biol.* 205:737–750.
66. Agashe, V. R., and J. B. Udgaonkar. 1995. Thermodynamics of denaturation of barstar: evidence for cold denaturation and evaluation of the interaction with guanidine hydrochloride. *Biochemistry*. 34:3286–3299.
67. Gómez, J., V. J. Hilser, ..., E. Freire. 1995. The heat capacity of proteins. *Proteins*. 22:404–412.
68. Wagner, G., and K. Wüthrich. 1982. Amide proton exchange and surface conformation of the basic pancreatic trypsin inhibitor in solution. Studies with two-dimensional nuclear magnetic resonance. *J. Mol. Biol.* 160:343–361.
69. Radford, S. E., M. Buck, ..., P. A. Evans. 1992. Hydrogen exchange in native and denatured states of hen egg-white lysozyme. *Proteins*. 14:237–248.
70. Chamberlain, A. K., T. M. Handel, and S. Marqusee. 1996. Detection of rare partially folded molecules in equilibrium with the native conformation of RNaseH. *Nat. Struct. Biol.* 3:782–787.
71. Clarke, J., and A. R. Fersht. 1996. An evaluation of the use of hydrogen exchange at equilibrium to probe intermediates on the protein folding pathway. *Fold. Des.* 1:243–254.
72. Bhuyan, A. K., and J. B. Udgaonkar. 1998. Two structural subdomains of barstar detected by rapid mixing NMR measurement of amide hydrogen exchange. *Proteins*. 30:295–308.
73. Riek, R., G. Wider, ..., K. Wüthrich. 1998. Prion protein NMR structure and familial human spongiform encephalopathies. *Proc. Natl. Acad. Sci. USA*. 95:11667–11672.
74. Tarus, B., J. E. Straub, and D. Thirumalai. 2006. Dynamics of Asp²³-Lys²⁸ salt-bridge formation in A β _{10–35} monomers. *J. Am. Chem. Soc.* 128:16159–16168.
75. De Simone, A., A. Dhulesia, ..., C. M. Dobson. 2011. Experimental free energy surfaces reveal the mechanisms of maintenance of protein solubility. *Proc. Natl. Acad. Sci. USA*. 108:21057–21062.
76. Lawson, V. A., S. A. Priola, ..., B. Chesebro. 2001. N-terminal truncation of prion protein affects both formation and conformation of abnormal protease-resistant prion protein generated in vitro. *J. Biol. Chem.* 276:35265–35271.
77. Béland, M., and X. Roucou. 2012. The prion protein unstructured N-terminal region is a broad-spectrum molecular sensor with diverse and contrasting potential functions. *J. Neurochem.* 120:853–868.
78. Jain, S., and J. B. Udgaonkar. 2008. Evidence for stepwise formation of amyloid fibrils by the mouse prion protein. *J. Mol. Biol.* 382:1228–1241.
79. Vendrely, C., H. Valadié, ..., M. Jamin. 2005. Assembly of the full-length recombinant mouse prion protein I. Formation of soluble oligomers. *Biochim. Biophys. Acta*. 1724:355–366.
80. Hornemann, S., and R. Glockshuber. 1996. Autonomous and reversible folding of a soluble amino-terminally truncated segment of the mouse prion protein. *J. Mol. Biol.* 261:614–619.
81. Privalov, P. L. 1979. Stability of proteins: small globular proteins. *Adv. Protein Chem.* 33:167–241.
82. Schellman, J. A. 1978. Solvent denaturation. *Biopolymers*. 17:1305–1322.
83. Schellman, J. A. 1987. The thermodynamic stability of proteins. *Annu. Rev. Biophys. Biophys. Chem.* 16:115–137.
84. Bolen, D. W., and M. M. Santoro. 1988. Unfolding free energy changes determined by the linear extrapolation method. 2. Incorporation of ΔG°_{N-U} values in a thermodynamic cycle. *Biochemistry*. 27:8069–8074.
85. Chen, B. L., and J. A. Schellman. 1989. Low-temperature unfolding of a mutant of phage T4 lysozyme. 1. Equilibrium studies. *Biochemistry*. 28:685–691.
86. Lee, B., and F. M. Richards. 1971. The interpretation of protein structures: estimation of static accessibility. *J. Mol. Biol.* 55:379–400.
87. Doig, A. J., and D. H. Williams. 1991. Is the hydrophobic effect stabilizing or destabilizing in proteins? The contribution of disulphide bonds to protein stability. *J. Mol. Biol.* 217:389–398.

Thermodynamic Characterization of the Unfolding of the Prion Protein

Supporting Material

Roumita Moulick and *Jayant B. Udgaonkar

National Centre for Biological Sciences

Tata Institute of Fundamental Research

Bangalore 560065, India

***Corresponding Author: Professor Jayant B. Udgaonkar**

Telephone: 080-23666150

Fax: 91-80-23636662

Email: jayant@ncbs.res.in

Funding Source Statement: This work was funded by the Tata Institute of Fundamental Research, and by the Department of Science and Technology, Government of India. JBU is the recipient of a J.C. Bose National Fellowship from the Government of India.

SUPPORTING MATERIAL

Materials and Methods:

Protein Expression & Purification

The full length recombinant mouse prion protein, moPrP (23-231), encoded in the pET-17b(+) plasmid was expressed in *Escherichia coli* BL21(DE3) codon plus (Stratagene) cells, and purified as described previously (9). The protein was transferred to 0.22- μm filtered water using an Amicon ultrafiltration cell and stored at $-80\text{ }^{\circ}\text{C}$. The concentration of the protein was determined by absorbance measurements at 280 nm using an extinction coefficient of $62,160\text{ M}^{-1}\text{ cm}^{-1}$ (10). The plasmid (pPrP-C) encoding the gene for the CTD, moPrP (121-231), was a gift from Prof. R. Glockshuber, and was expressed in *Escherichia coli* BL21(DE3) codon plus (Stratagene) cells. moPrP (121-231) was purified as described previously (11). The protein was dialyzed against 0.22- μm filtered water and stored at -80°C . The concentration of the protein was determined by absorbance measurements at 280 nm using an extinction coefficient of $19890\text{ M}^{-1}\text{ cm}^{-1}$ (1). The purity of moPrP (23-231) as well as of moPrP (121-231) was confirmed by SDS-PAGE and mass spectrometry using a Synapt G2 mass spectrometer from Waters. The masses of moPrP (23-231) and moPrP (121-231) were 23,236 Da and 13,334 Da respectively.

Chemicals and Buffers

All the experiments utilized buffers containing 20 mM sodium acetate adjusted to pH 4, and variable concentrations of urea (obtained from USB) in the range 0-8 M. All solutions were filtered using 0.22- μm Millipore syringe filters before use. The concentrations of urea stock solutions prior to use were determined by refractive index measurements using an Abbe refractometer. All chemicals used were obtained from Sigma (unless mentioned otherwise).

Urea-induced Denaturation

Isothermal urea-induced equilibrium unfolding was monitored by far-UV CD measurements done on a Jasco J815 spectropolarimeter. Secondary structure measurements were made at 222 nm using a 0.1 cm path length cuvette, 1 nm bandwidth and averaged over two minutes. The sample temperature was maintained by a Peltier temperature controller (PTC-423L) from Jasco.

Thermal Denaturation

Thermally induced equilibrium unfolding was monitored by measurement of the change in mean residual ellipticity at 222 nm using a Jasco J815 spectropolarimeter. Temperature was ramped using the PTC-423L. The protein concentration employed was 10 μM , in a 0.1 cm path length cuvette. Heating rates of 0.5 K/min below $20\text{ }^{\circ}\text{C}$ and 1 K/min above $20\text{ }^{\circ}\text{C}$ were used. The temperature in the cuvette was monitored using a Jasco pyrometer with an accuracy of $\pm 0.5\text{ K}$. Reversibility of thermal denaturation was checked by cooling the thermally denatured protein on

ice and rescanning. This was done to avoid chemical modifications to the protein due to long exposure to high temperature.

Differential Scanning Calorimetric Measurements

Differential scanning calorimetry measurements of the two proteins were done using a Microcal VP-DSC calorimeter, using protein concentrations of 15 and 20 μM for full length and CTD respectively, in 20 mM sodium acetate buffer at pH 4. A scan rate of 1K/min was used.

Determination of Absolute Native state heat capacity

moPrP (121-231) was dialyzed extensively against 20 mM NaOAc, pH 4 and then diluted to different protein concentrations ranging from 10 to 30 μM . In a typical measurement, the sample and reference calorimetric cells were filled with the dialysis buffer from the last dialysis step, and the heat capacity of the sample cell measured as a continuous function of temperature, with respect to the solution in reference cell, repeatedly till a stable baseline is achieved. Next, the sample cell was emptied of the buffer, and protein solution was loaded keeping the calorimeter in same thermal cycle. After measurement of heat capacity at any protein concentration, the sample cell was rinsed thoroughly with buffer, and then protein of a higher concentration was loaded. Thus, the heat capacity of five concentrations of moPrP (121-231) was measured. The exact concentration of protein in each sample was estimated by an absorbance measurement after the DSC scan was over. In all cases, remarkable reversibility was observed and the thermodynamic parameters were found to be similar within experimental error to that obtained from thermal scans monitored by circular dichroism.

Data Analysis

For a two-state $N \leftrightarrow U$ unfolding reaction characterized by a change in heat capacity, ΔC_p , which is independent of temperature over the range of temperature measurements (12), the thermodynamic equations for the dependence of the changes in enthalpy (ΔH), entropy (ΔS), and free energy (ΔG) on temperature in the absence of any denaturant are given below:

$$\Delta G = \Delta H - T\Delta S \quad (\text{S1})$$

$$\Delta H(T) = \Delta H_g + \Delta C_p(T - T_g) \quad (\text{S2})$$

$$\Delta S(T) = \Delta S_g + \Delta C_p \ln(T/T_g) \quad (\text{S3})$$

$$\Delta G(T) = \Delta H_g \left(1 - \frac{T}{T_g}\right) + \Delta C_p \left(T - T_g - T \ln\left(\frac{T}{T_g}\right)\right) \quad (\text{S4})$$

T_g , the midpoint of the thermal transition, and therefore the temperature at which $\Delta G(T) = 0$, is taken as the reference temperature. ΔH_g and ΔS_g are the values of ΔH and ΔS at T_g .

According to the linear free energy model (4,8,13-16), the changes in free energy, enthalpy, entropy and heat capacity during unfolding in the presence of denaturant, denoted here by $\Delta G'$, $\Delta H'$, $\Delta S'$ and $\Delta C'_p$, respectively, all have linear dependences on the concentration of denaturant [D]:

$$\Delta G' = \Delta G + \Delta G_i[D] \quad (\text{S5A})$$

$$= \Delta G + m_G[D] \quad (\text{S5B})$$

$$\Delta H' = \Delta H + \Delta H_i[D] \quad (\text{S6})$$

$$\Delta S' = \Delta S + \Delta S_i[D] \quad (\text{S7})$$

$$\Delta C'_p = \Delta C_p + \Delta C_{p_i}[D] \quad (\text{S8})$$

$$\Delta G_i = \Delta H_i - T\Delta S_i \quad (\text{S9})$$

$$\Delta G' = \Delta H' - T\Delta S' \quad (\text{S10})$$

ΔG_i (m_G), ΔH_i , ΔS_i and ΔC_{p_i} are the preferential free energy, enthalpy, entropy and heat capacity, respectively, of interaction of denaturant with the unfolded form of the protein relative to with the folded form. The denaturant concentration at which the protein is half unfolded ($\Delta G=0$) under isothermal conditions is denoted as C_m and from Eq. S5, $\Delta G = -C_m m_G$.

With the assumption that ΔC_{p_i} is independent of temperature (12), the temperature dependences of ΔH_i , ΔS_i and ΔG_i are given by:

$$\Delta H_i(T) = \Delta H_i^0 + \Delta C_{p_i}(T - T^0) \quad (\text{S11})$$

$$\Delta S_i(T) = \Delta S_i^0 + \Delta C_{p_i} \ln(T/T^0) \quad (\text{S12})$$

$$\Delta G_i(T) = \Delta H_i^0 - T\Delta S_i^0 + \Delta C_{p_i}(T - T^0 - T \ln(T/T^0)) \quad (\text{S13})$$

ΔH_i^0 and ΔS_i^0 are the values of ΔH_i and ΔS_i at a reference temperature T^0 , which may be set to T'_g . Thus, the temperature dependences of $\Delta H'$, $\Delta S'$ and $\Delta G'$ are as follows:

$$\Delta H'(T) = \Delta H'_g + \Delta C'_p(T - T'_g) \quad (\text{S14})$$

$$\Delta S'(T) = \Delta S'_g + \Delta C'_p \ln(T/T'_g) \quad (\text{S15})$$

$$\Delta G'(T) = \Delta H'_g \left(1 - \frac{T}{T'_g}\right) + \Delta C'_p \left(T - T'_g - T \ln \left(\frac{T}{T'_g}\right)\right) \quad (\text{S16})$$

Where T'_g is the midpoint of the thermal transition in the presence of denaturant where $\Delta G'=0$.

Composite stability curves in the absence and presence of denaturant (Fig. 4) were fit to Eq. S4 and Eq. S16, respectively, to obtain the values of $\Delta H'_g$, T'_g and $\Delta C'_p$.

$\Delta H'_g$, estimated from a fit of stability curves to Eq. S16 was corrected for the contribution of $\Delta H'_1$ at T'_g according to Eq. S17:

$$\Delta H'_{g \text{ cor}} = \Delta H'_g(\text{observed}) - \Delta H'_i(T'_g) \cdot [D] \quad (\text{S17})$$

$\Delta H'_{g \text{ cor}}$ is the actual enthalpy change during the unfolding reaction. The slope of a plot of $\Delta H'_{g \text{ cor}}$ versus T'_g gives $\Delta C'_p$.

Isothermal Denaturant-induced Unfolding

A denaturant-induced unfolding transition at a given temperature was analyzed in two different ways to obtain ΔG at that particular temperature. In the first method of analysis, the equilibrium unfolding data was directly fit to a two-state $N \leftrightarrow U$ unfolding model using Eq. S18 (8, 15):

Y_0

$$= \frac{\left[Y_F + m_F[D] + (Y_U + m_U[D]) \exp \left[\frac{-\Delta G + m_G[D]}{RT} \right] \right]}{\left[1 + \exp \left[\frac{-\Delta G + m_G[D]}{RT} \right] \right]} \quad (\text{S18})$$

Y_0 is the CD value at a particular denaturant concentration, Y_F and Y_U represent the intercepts, and m_F and m_U the slopes of the native and unfolded protein baselines, respectively. In the second method of analysis, the raw data was converted into fraction unfolded values using Eq. S19:

$$f_U = \frac{[Y_0 - (Y_F + m_F[D])]}{[(Y_U + m_U[D]) - (Y_F + m_F[D])]} \quad (\text{S19})$$

f_U is related to the equilibrium constant, K_{app} by the relationship: $K_{\text{app}} = f_U / (1 - f_U)$ which is further related to the free energy as $\Delta G = -RT \ln K_{\text{app}}$. Hence, f_U is related to ΔG by a transformation of the Gibbs-Helmholtz Eq. as:

f_U

$$= \frac{\exp \left[-\frac{\Delta G + m_G[D]}{RT} \right]}{\left[1 + \exp \left[-\frac{\Delta G + m_G[D]}{RT} \right] \right]} \quad (\text{S20})$$

Thermally induced unfolding

Thermally induced unfolding transitions in the presence and absence of denaturant were used to determine the apparent equilibrium constant, K_{app} and the free energy change, $\Delta G'$ at any temperature using the following equations:

$$K_{app} = \frac{f_U}{1 - f_U} = \frac{Y_0 - (Y_F + m_F T)}{(Y_U + m_U T) - Y_0} \quad (S21)$$

$$\Delta G' = -RT \ln K_{app} = -RT \ln \left(\frac{Y_0 - (Y_F + m_F T)}{(Y_U + m_U T) - Y_0} \right) \quad (S22)$$

Y_0 is the mean residue ellipticity measured at temperature, T in the presence of denaturant at concentration, $[D]$. Y_F and Y_U are the intercepts and m_F and m_U the slopes of the native and unfolded protein base lines, respectively. The values of K_{app} in the folding transition zone were used to determine $\Delta G'$ as a function of T . T'_g was obtained as the temperature at which $\Delta G'=0$. $\Delta S'_g$, the change in entropy associated with the unfolding reaction at T'_g , was estimated either from a plot of $\Delta G'$ versus T at T'_g , whose slope, $\Delta H'_g/T'_g$ is equal to $\Delta S'_g$ (Eq. S16), or from a van't Hoff plot of $\ln K_{app}$ versus $1/T$ whose slope is $-\Delta H'_g/R$. The two estimates were found to be essentially in agreement with each other.

Thermally induced unfolding transitions in the presence of denaturant are described by:

Y_0

$$= \frac{(Y_F + m_F T) + (Y_U + m_U T) \times \exp \left[\frac{\Delta H'_g \left(\frac{T}{T'_g} - 1 \right) + \Delta C'_p \left[T'_g - T + T \ln \left(\frac{T}{T'_g} \right) \right]}{RT} \right]}{1 + \exp \left[\frac{\Delta H'_g \left(\frac{T}{T'_g} - 1 \right) + \Delta C'_p \left[T'_g - T + T \ln \left(\frac{T}{T'_g} \right) \right]}{RT} \right]} \quad (S23)$$

Fraction unfolded, f_U , versus T plots of thermally induced unfolding transitions were also constructed according to equation:

$$f_U = \frac{\exp\left[\frac{\Delta H'_g \left(\frac{T}{T'_g} - 1\right) + \Delta C'_p \left[T'_g - T + T \ln\left(\frac{T}{T'_g}\right)\right]}{RT}\right]}{1 + \exp\left[\frac{\Delta H'_g \left(\frac{T}{T'_g} - 1\right) + \Delta C'_p \left[T'_g - T + T \ln\left(\frac{T}{T'_g}\right)\right]}{RT}\right]} \quad (\text{S24})$$

A thermally induced unfolding transition in the absence of denaturant is described by Eqs. S23 and S24 with ΔH_g , T_g and ΔC_p as the parameters instead of $\Delta H'_g$, T'_g and $\Delta C'_p$.

The temperature dependence of unfolding in the absence of denaturant is characterized by the temperatures T_h , T_s and T_g (13,14) at which ΔH , ΔS and ΔG equal to 0, respectively. These characteristic temperatures are related to each other as:

$$T_h = T_g - \frac{\Delta H_g}{\Delta C_p} \quad (\text{S25})$$

$$\ln(T_g/T_s) = \frac{\Delta H_g}{\Delta C_p T_g} \quad (\text{S26})$$

$$\Delta G_s = \Delta C_p (T_s - T_h) \quad (\text{S27})$$

Differential Scanning Calorimetry measurements

DSC data were fit using the Origin DSC software provided by Microcal Inc. Baseline buffer versus buffer scans were first subtracted from protein versus buffer scans. The resultant buffer corrected scans were normalized to protein concentration and fit to a two-state unfolding model assuming the transition to be a two-state process. The area under the curve gives an estimate of the total change in enthalpy, ΔH_{cal} during the unfolding transition, and the change in heat capacity, ΔC_p was estimated by extrapolating the native and unfolded protein baselines to T_g , the midpoint of thermal transition, and determining the difference in values at T_g .

The van't Hoff enthalpy, ΔH_{vH} was calculated using Eq. S28 (12).

$$\Delta H_{\text{vH}} = 4RT_g^2 \left[\frac{\Delta C_p^{\text{max}}}{Q} \right] \quad (\text{S28})$$

Here, Q is the total heat of denaturation or the area under the peak which is ΔH_{cal} . ΔC_p^{max} is the heat capacity at T_g obtained from the peak.

Calculation of absolute heat capacity of the native state

The absolute heat capacity of the native state of moPrP (121-231) was estimated as reported by Kholodenko, 1999 (2). The partial volume was taken to be 0.730 mL g⁻¹ (3) and the cell volume was ~0.5 mL. Prior to baseline subtraction, the measured heat capacity, C_p , may be written as in Eq. S29.

$$C_P = m_P \cdot C_{P,p} + m_b \cdot C_{P,b} + C_{P,ref} \quad (S29)$$

where $C_{P,p}$ and $C_{P,b}$ are the specific heat capacities of protein and buffer respectively and m_P and m_b are the mass of protein and buffer in sample cell. $C_{P,ref}$ is the contribution of the heat capacity of the buffer in the reference cell, difference in heat capacities between the cells and other instrument components, combined. Since, the volume of the cell is constant, Eq.S29 may be rewritten as:

$$\begin{aligned} C_P &= m_P \cdot C_{P,p} + \rho_b \cdot (v_0 - v_P \cdot m_P) C_{P,b} + C_{P,ref} \\ &= C_{P,b} \cdot \rho_b \cdot v_0 + (C_{P,p} - v_P \cdot C_{P,b} \cdot \rho_b) m_P + C_{P,ref} \end{aligned} \quad (S30)$$

Here, ρ_b is the density of the solution, v_0 is the volume of the cell and v_P is the partial volume of the protein. The slope, $\partial C_P / \partial m_P$ is sufficient to calculate C_P as for dilute solutions, $C_{P,b} \cdot \rho_b \sim 1 \text{ cal K}^{-1} \text{ mL}^{-1}$. For globular proteins, the average partial volume is 0.730 mL g^{-1} (3).

Accessible Surface Area calculations

The program PSA which implements the algorithm of Lee and Richards (17) was used to compute the solvent-accessible surface areas (ASA) of moPrP and 45 other proteins, as listed in a previous study (7). For moPrP, the pdb entry 1AG2 was used. Residue ASA's for different globular proteins were calculated using a probe radius of 1.4 \AA and slice width of 0.05 \AA . Here, C_α of the peptide backbone was considered to be aliphatic while the CO-NH part of the peptide backbone was considered to be polar. S atom was considered to be polar. In the case of aromatic residues, contributions to ΔASA_{arm} from the C_β atom onwards have been considered, while the polar part in an aromatic residue have been considered to be polar. The ASA value for each residue type in the unfolded protein was found by the tripeptide (AXA) method, and the ΔASA for each residue was calculated accordingly. Summation over all residues gave the total ΔASA for a protein. The dependence of ΔASA on the number of residues was in good agreement with that reported previously.

In Fig. S9, the changes in non-polar accessible surface area were corrected for the effect of disulphide bonds (when present in the protein) as disulphide bonds are known to reduce solvent accessibility in the unfolded polypeptide chain. An average correction factor of $630 \text{ \AA}^2/\text{disulphide bond}$ was used as from previous studies (4, 18).

Enthalpy and Entropy of hydration calculations:

The enthalpy of hydration may be represented as (5):

$$\Delta H^{hyd} = \Delta H_{pol}^{hyd} + \Delta H_{npl}^{hyd}$$

where

$$\Delta H_{pol}^{hyd} = \sum_i (\Delta \hat{H}_i^{hyd} * \Delta ASA_{pol})$$

$$\Delta H_{npl}^{hyd} = \sum_i (\Delta \hat{H}_{arm}^{hyd} * \Delta ASA_{arm} + \Delta \hat{H}_{alp}^{hyd} * \Delta ASA_{alp})$$

Here, *i* is an amino acid, ΔASA_{pol} is the total change in accessible surface area of the polar part of *i* upon unfolding and $\Delta \hat{H}_i^{hyd}$ is enthalpy of hydration per unit change in area for polar part of *i*. ΔASA_{arm} and ΔASA_{alp} are the total change in accessible surface area of the aromatic (if any) and aliphatic parts of amino acids upon unfolding and $\Delta \hat{H}_{arm}^{hyd}$ and $\Delta \hat{H}_{alp}^{hyd}$ are the enthalpy of hydrations per unit change in area for aromatic and aliphatic parts of *i*, respectively. Similarly, the entropy of hydration may be represented as (6):

$$\Delta S^{hyd} = \Delta S_{pol}^{hyd} + \Delta S_{npl}^{hyd}$$

where

$$\Delta S_{pol}^{hyd} = \sum_i (\Delta \hat{S}_i^{hyd} * \Delta ASA_{pol})$$

$$\Delta S_{npl}^{hyd} = \sum_i (\Delta \hat{S}_{arm}^{hyd} * \Delta ASA_{arm} + \Delta \hat{S}_{alp}^{hyd} * \Delta ASA_{alp})$$

The values for the enthalpy and entropy of hydration for the polar, aromatic and aliphatic parts of amino acid residues per unit change in accessible surface area were obtained from the enthalpies and entropies of transfer of simple organic compounds from the gaseous phase to water assuming that each group contributes additively to the overall enthalpy and entropy of transfer for the entire protein molecule (5, 6).

SUPPLEMENTARY TEXT

Dependence of the thermodynamic parameters of unfolding of moPrP on protein concentration

Fig. S1 shows urea-induced unfolding curves at 40 °C as well as thermally induced unfolding curves both in the absence and presence of 3 M urea, for 5, 10 and 20 μ M moPrP (23-231). In all cases, the unfolding curves were identical at all three protein concentrations: the melts at the different protein concentrations overlapped on top of each other. This indicates that equilibrium unfolding of moPrP is independent of protein concentration in the concentration range 5-20 μ M. The complete reversibility of unfolding under all conditions, as well as the independence of the unfolded baselines to concentration of protein which is evident in Fig. S1d, e and f, indicates that the protein does not oligomerize during unfolding.

Urea dependence of unfolded state mean residual ellipticity

Fig. S2 shows the dependence of mean residual ellipticity of unfolded state on urea at 360 K monitored at 222 nm. The mean residual ellipticity increases with increase in denaturant concentration but no cooperative transition is observed (see Discussion).

Denaturant dependence of enthalpy, entropy and free energy changes upon unfolding

The data shown in Fig. 4 and Table 1 were used for a detailed analysis of the dependences of the changes in enthalpy, $\Delta H'$, entropy, $\Delta S'$ and heat capacity, $\Delta C'_p$ associated with unfolding, on denaturant concentration at temperatures ranging from 276 K to 313 K. Fig. S3a shows the dependence of $\Delta H'$ on urea concentration at three different temperatures. $\Delta H'$ is seen to be more favourable at lower temperatures. At each temperature, $\Delta H'$ is observed to decrease linearly with an increase in urea concentration indicating that the protein interacts favourably with the denaturant. Fig. S3b shows that the magnitude of $\Delta S'$ becomes increasingly negative with an increase in urea concentration indicating an unfavourable interaction. Fig. S3c shows that $\Delta G'$ decreases linearly with increasing concentration of urea, with a slope, ΔG_i , which is the contribution to the free energy change due to preferential interaction of urea with the unfolded form relative to with the native form. The values of $\Delta G'$ at all temperatures and denaturant concentrations are in good agreement with the values obtained from the urea-induced denaturation curves, and the linear dependences of $\Delta G'$ on urea concentration predict the values of ΔG at zero urea concentration at all temperatures as shown in Fig. S3c.

Temperature dependences of ΔH_i , ΔS_i and ΔG_i

The slopes of the linear dependences of $\Delta H'$, $\Delta S'$ and $\Delta G'$ on urea concentration at each temperature yield the values of ΔH_i , ΔS_i and ΔG_i , respectively, at that temperature according to Eqs. S5-S7. Fig. S4a, b and c show the temperature dependences of ΔH_i , ΔS_i and ΔG_i respectively, as described by Eqs. S11-S13. ΔG_i is the same as m_G (see Eqs. S5a and S5b) and the magnitudes of ΔG_i are in good agreement with the values of m_G listed in Table S1.

Dependences of T'_g , T'_h and T'_s on urea concentration

Fig. S5 shows the dependences of T'_g , T'_h and T'_s , whose values were determined using Eq. S25 and Eq. S26, on urea concentration. The midpoint of thermal denaturation, T'_g , decreases with a decrease in the stability of the protein with increasing concentration of urea as expected.

Urea-induced unfolding of moPrP at pH 7, and at pH 4 in the presence of salt

Fig. S6a shows differential stability of moPrP (23-231) and moPrP (121-231) at pH 7. Fig. S6b shows that moPrP (23-231) converts into an oligomer at pH 4 in the presence of high concentration of salt (see Discussion).

Delineation of the contributions of hydration and internal interactions to individual thermodynamic parameters.

Fig. S7 shows the change of hydration enthalpy and entropy per residue and enthalpy and entropy of intramolecular interactions per residue for the six proteins (see Discussion).

Temperature dependences of the hydration of polar and non-polar groups during unfolding

The contribution of polar and non-polar groups to the hydration enthalpy, entropy and free energy were delineated using surface area calculations as described above (Fig. S8).

Heat capacity change for the unfolding of moPrP (121-231) compared to other globular proteins

In Fig. S9, the change in heat capacity per residue upon unfolding is plotted against the average non-polar surface area, ΔASA_{npI} per residue that becomes exposed to water upon unfolding, taking into account the effect of any disulphide(s) present (see Methods). The value for moPrP (121-231) (□) is compared to the values for forty other proteins as listed in Robertson and Murphy (7). The value of $\Delta C_P/N_R$ for moPrP (121-231) is half of that expected for a protein undergoing a similar change in its average non-polar accessible surface area upon unfolding.

SUPPLEMENTAL TABLES:

Table S1: Parameters governing the urea-induced unfolding of the mouse prion protein at pH 4

Temperature (K)	ΔG (kcal mole ⁻¹)	m_G (kcal mole ⁻¹ M ⁻¹)	C_m (M)	ΔG (kcal mole ⁻¹)	m_G (kcal mole ⁻¹ M ⁻¹)	C_m (M)
276	5.9	1.6	3.7	5.8	1.5	3.8
283	5.4	1.5	3.7	5.7	1.5	3.7
288	5.4	1.5	3.7	5.7	1.5	3.6
293	5.3	1.5	3.6	5.1	1.4	3.5
298	4.8	1.5	3.4	5.1	1.5	3.3
303	4.8	1.4	3.2	4.5	1.4	3.3
308	4.5	1.4	3.0	3.9	1.3	3.2
313	3.7	1.2	3.0	3.6	1.2	3.0

Individual errors in the determination of the thermodynamic parameters are not shown for the sake of clarity. Errors in ΔG values were typically ± 0.3 kcal mole⁻¹. Errors in m_G values were typically ± 0.1 kcal mole⁻¹M⁻¹. Errors in C_m values were typically ± 0.1 M.

Table S2: Enthalpy and entropy of denaturation of mouse prion protein at pH 4

Temperature (K)	278	298	323	348	373	398
${}^a\Delta H$ (kcal mole ⁻¹ res ⁻¹)	0.1	0.2	0.4	0.6	0.8	0.9
${}^a\Delta S$ (cal K ⁻¹ mole ⁻¹ res ⁻¹)	0.2	0.7	1.3	1.8	2.3	2.8
${}^b\Delta H^{\text{hyd}}$ (kcal mole ⁻¹ res ⁻¹)	-17.4	-17.2	-16.9	-16.6	-16.3	-16
${}^b\Delta S^{\text{hyd}}$ (cal K ⁻¹ mole ⁻¹ res ⁻¹)	-18	-17.2	-16.2	-15.3	-14.5	-13.8
${}^c\Delta H^{\text{int}}$ (kcal mole ⁻¹ res ⁻¹)	17.5	17.4	17.3	17.2	17.1	17.0
${}^c\Delta S^{\text{int}}$ (cal K ⁻¹ mole ⁻¹ res ⁻¹)	18.1	17.8	17.4	17.1	16.8	16.5

${}^a\Delta H$ and ΔS are the experimentally determined values of the enthalpy and entropy of unfolding. $\Delta H = \Delta H^{\text{hyd}} + \Delta H^{\text{int}}$, and $\Delta S = \Delta S^{\text{hyd}} + \Delta S^{\text{int}}$, where ΔH^{hyd} and ΔS^{hyd} are the calculated enthalpy and entropy of hydration of both polar and non-polar parts of residues upon unfolding(5,6).

${}^b\Delta H^{\text{hyd}} = \Delta H_{\text{pol}}^{\text{hyd}} + \Delta H_{\text{npl}}^{\text{hyd}}$ where $\Delta H_{\text{pol}}^{\text{hyd}}$ is the contribution of polar parts of residues and $\Delta H_{\text{npl}}^{\text{hyd}}$ is the contribution of non-polar parts of residues to ΔH^{hyd} . $\Delta H_{\text{pol}}^{\text{hyd}}$ and $\Delta H_{\text{npl}}^{\text{hyd}}$ are directly proportional to the changes in polar surface area ($\Delta\text{ASA}_{\text{pol}}$) and non-polar surface area ($\Delta\text{ASA}_{\text{npl}}$), respectively, and were determined from model compound data (5) and the values were determined for $\Delta\text{ASA}_{\text{pol}}$ (4989 Å²) and $\Delta\text{ASA}_{\text{npl}}$ (6069 Å²) for the moPrP (121-231). ΔS^{hyd} was determined similarly using model compound data (6).

${}^c\Delta H^{\text{int}}$ and ΔS^{int} were determined by subtracting ΔH^{hyd} and ΔS^{hyd} from ΔH and ΔS .

SUPPLEMENTAL FIGURES:

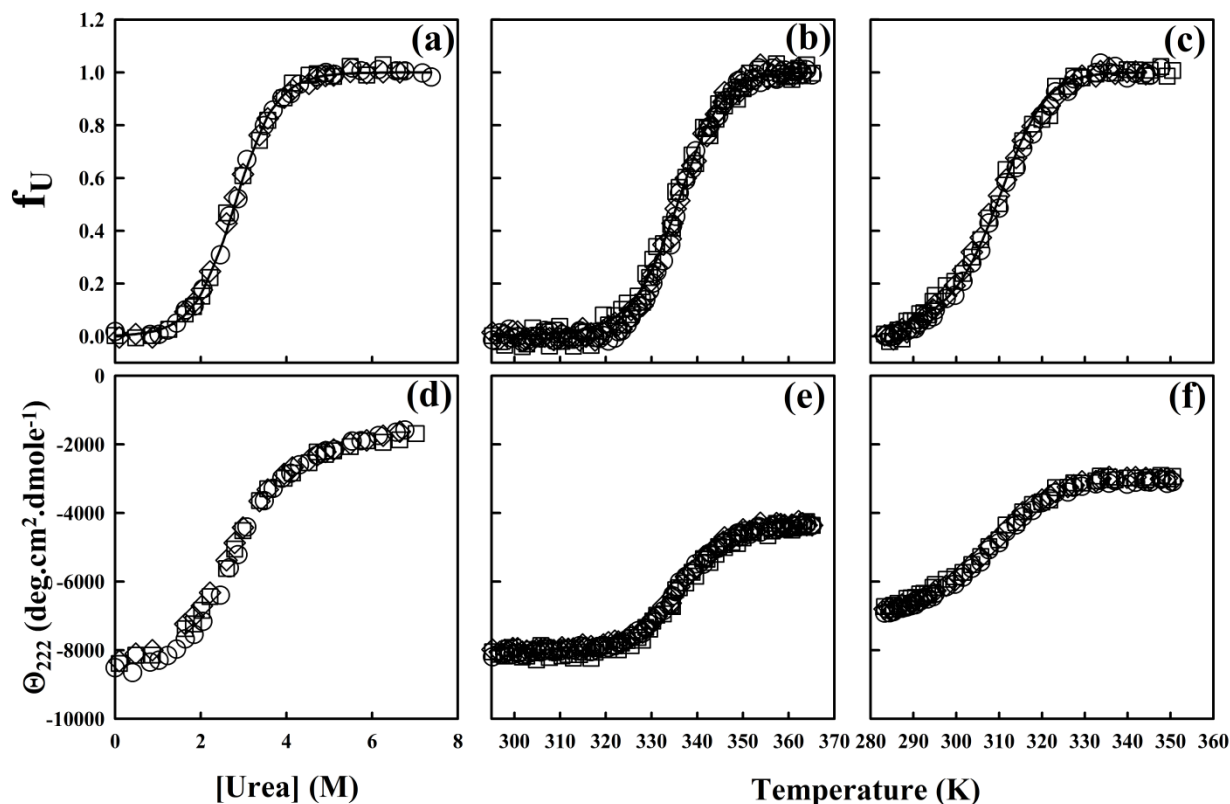


Figure S1. Dependence of the stability of moPrP at pH 4 on protein concentration determined from isothermal urea-induced and thermally induced equilibrium unfolding curves. (a) Fraction of protein in the unfolded form, f_U , determined by Eq. S19 is plotted against the concentration of urea at 313 K for 5 (\square), 10 (\circ) and 20 (\diamond) μM moPrP (23-231). The solid line through the data is a fit of 20 μM data to Eq. S20. Fig. S1(d) shows the corresponding dependence of the mean residual ellipticity (MRE) at 222 nm on urea concentration. Thermally induced unfolding transitions in the absence (b) and in the presence (c) of 3 M urea are shown for 5 (\square), 10 (\circ) and 20 (\diamond) μM moPrP (23-231). The fraction of protein in the unfolded form, f_U , is plotted against temperature. The solid lines through the data are non-linear least-squares fits of the 20 μM data to Eq.S24. Fig. S1e and f show the corresponding MRE plots. The overlapping MRE plots show that the unfolded protein baselines are independent of protein concentration.

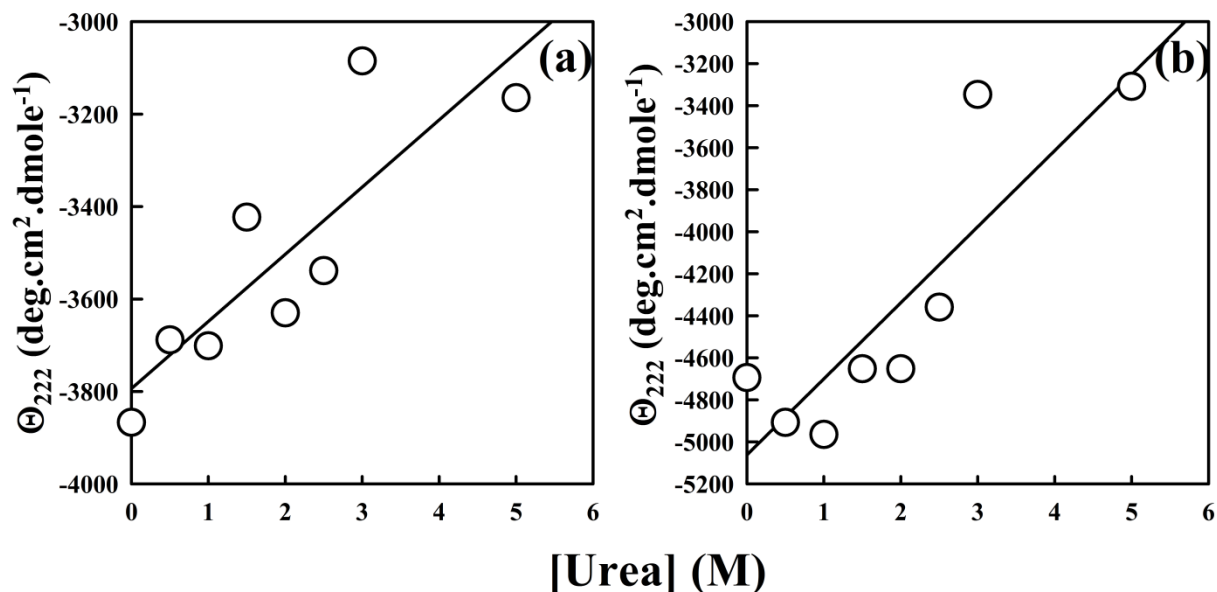


Figure S2. Urea dependence of mean residual ellipticity at 222 nm at 360 K. The mean residual ellipticity was obtained from thermal denaturation curves at different denaturant concentration for moPrP (23-231) and moPrP (121-231) as shown in (a) and (b) respectively. The mean residual ellipticity varies by less than 5% as observed from multiple denaturation curves. The straight line through the data in (a) and (b) are linear least squares fit to the data with slopes of 145 deg.cm².dmole⁻¹ M⁻¹ and 362 deg.cm².dmole⁻¹ M⁻¹ respectively.

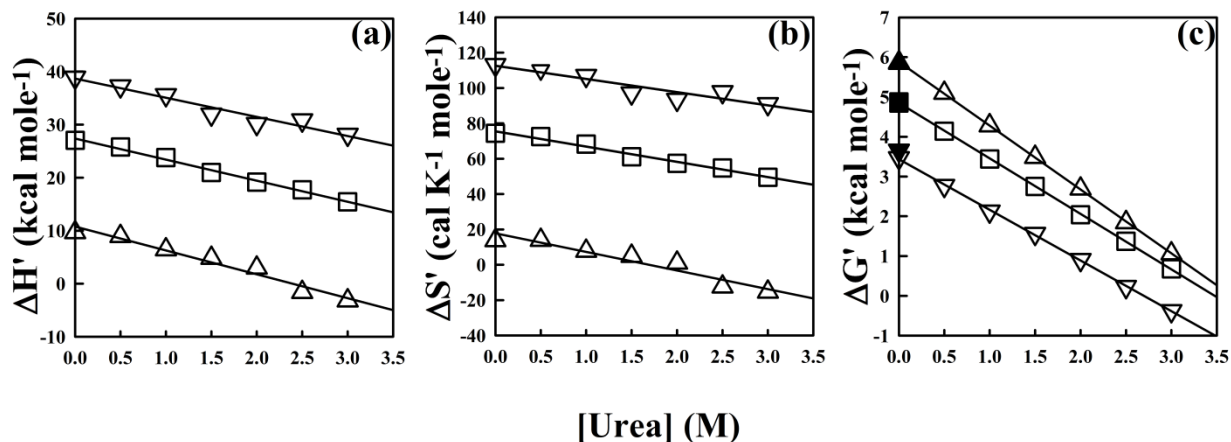


Figure S3. Urea dependence of $\Delta H'$, $\Delta S'$ and $\Delta G'$ at pH 4. The values of $\Delta H'$, $\Delta S'$ and $\Delta G'$ were determined at temperatures 276 K (\blacktriangle), 298 K (\square) and 313 K (∇) for each concentration of urea using Eqs. S14-S16. The values for $\Delta H'_g$, $\Delta S'_g$, $\Delta C'_p$ and T'_g are listed in Table 1. (a), (b) and (c) show the dependences of $\Delta H'$, $\Delta S'$ and $\Delta G'$ at 276 K, 298 K and 313 K on urea concentration. In (c), the filled symbols denote the values of ΔG determined from isothermal urea-induced unfolding transitions. The straight lines through the data in (a), (b) and (c) are linear least-squares fits to Eqs. S6, S7 and S5A, respectively. The intercepts and slopes of the fitted lines yield the values for ΔH and ΔH_i of 10.8 ± 0.7 kcal mole $^{-1}$ and -4.5 ± 0.4 kcal mole $^{-1}M^{-1}$, ΔS and ΔS_i of 17.7 ± 2.4 cal K $^{-1}$ mole $^{-1}$ and -10.5 ± 1.3 cal K $^{-1}$ mole $^{-1}M^{-1}$, ΔG and ΔG_i of 5.88 ± 0.02 kcal mole $^{-1}$ and -1.6 kcal mole $^{-1}M^{-1}$ at 276 K; ΔH and ΔH_i of 38.7 ± 0.7 kcal mole $^{-1}$ and -3.6 ± 0.4 kcal mole $^{-1}M^{-1}$, ΔS and ΔS_i of 112.5 ± 2.3 cal K $^{-1}$ mole $^{-1}$ and -7.5 ± 1.3 cal K $^{-1}$ mole $^{-1}M^{-1}$, and ΔG and ΔG_i of 3.44 ± 0.02 kcal mole $^{-1}$ and -1.3 ± 0.01 kcal mole $^{-1}M^{-1}$ at 313K. At 298K, the ΔH , ΔH_i , ΔS and ΔS_i values are 27.4 ± 0.3 kcal mole $^{-1}$, -4.0 ± 0.2 kcal mole $^{-1}M^{-1}$, 75.5 ± 0.9 cal K $^{-1}$ mole $^{-1}$ and -8.7 ± 0.5 cal K $^{-1}$ mole $^{-1}M^{-1}$ and ΔG , ΔG_i values are 4.85 ± 0.01 kcal mole $^{-1}$ and -1.4 ± 0.01 kcal mole $^{-1}M^{-1}$.

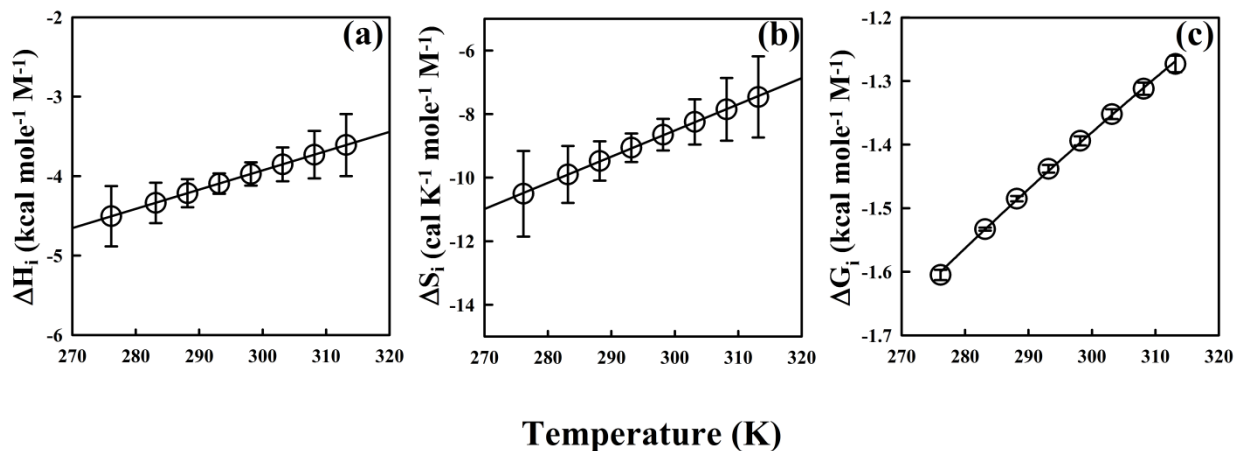


Figure S4. Dependence of the thermodynamic parameters governing the interaction of the mouse prion protein with urea at pH 4 on temperature. (a) shows the dependence of ΔH_i on temperature. The straight line through the data is a linear, least-squares fit of the data to Eq. S11, whose slope, ΔC_{P_i} equals to $24 \text{ cal K}^{-1} \text{ mole}^{-1} \text{ M}^{-1}$. (b) shows the dependence of ΔS_i on temperature. The line through the data is a least-squares fit of the data to Eq. S12. Fig. S4c shows the dependence of ΔG_i on temperature. The line through the data is a least-squares fit of the data to Eq. S13. The errors shown in the values of ΔH_i , ΔS_i and ΔG_i are the standard errors obtained from the least-squares fits shown in Fig. S3.

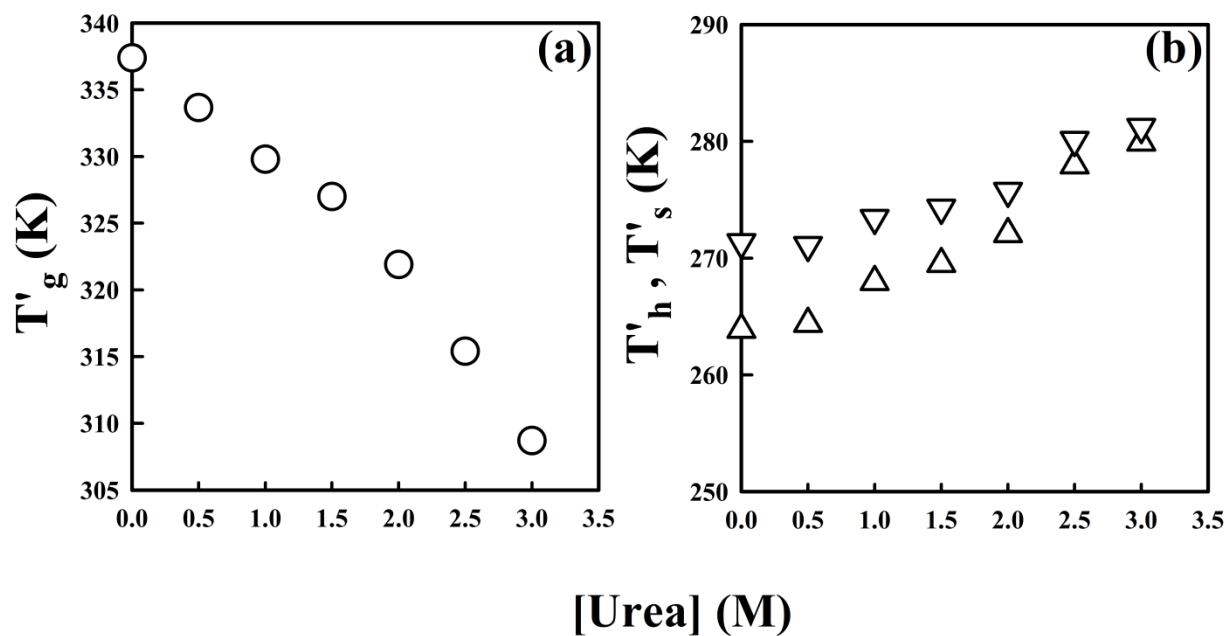


Figure S5. Dependences of T'_h , T'_s and T'_g of mouse prion protein at pH 4 on urea concentration. (a) shows the dependence of T'_g (\circ), and (b) shows the dependences of T'_h (\triangle) and T'_s (∇) on urea concentration. The values for the characteristic temperatures are listed in Table 1.

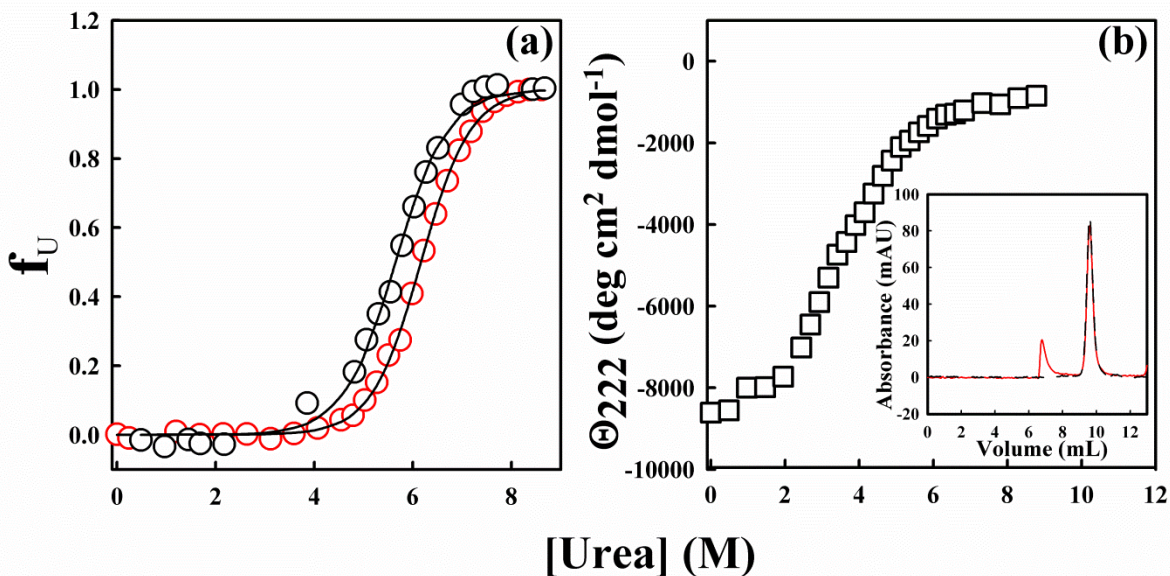


Figure S6. Oligomerization of moPrP (23-231) at pH 4 in the presence of salt. (a) shows urea-induced denaturation curves at 295 K at pH 7 for moPrP (23-231) (○) and moPrP (121-231) (○). The fraction of protein in the unfolded form determined using Eq. S19, is plotted against the concentration of urea at 295 K. The solid lines through the data are non-linear least-squares fits of the data to Eq. S20 and yield values for ΔG , m_G and C_m of 6.1 kcal mole⁻¹, 1.1 kcal mole⁻¹ M⁻¹ and 5.6 M for moPrP (23-231), and 7.3 kcal mole⁻¹, 1.2 kcal mole⁻¹ M⁻¹ and 5.8 M for moPrP (121-231). (b) shows the urea-induced denaturation curve at 298 K at pH 4 for moPrP (23-231) with 100 mM NaCl present in 20 mM NaOAc buffer at 120 h (□) of equilibration. The inset shows the size exclusion profile of protein in 3.6 M urea at 120 h of equilibration in the absence (dashed line in black) and in the presence (solid line in red) of 100 mM NaCl. Monomeric protein elutes out at 10 mL, while oligomer elutes out at 6 mL. Unfolded protein does not elute out as it sticks to the column matrix.

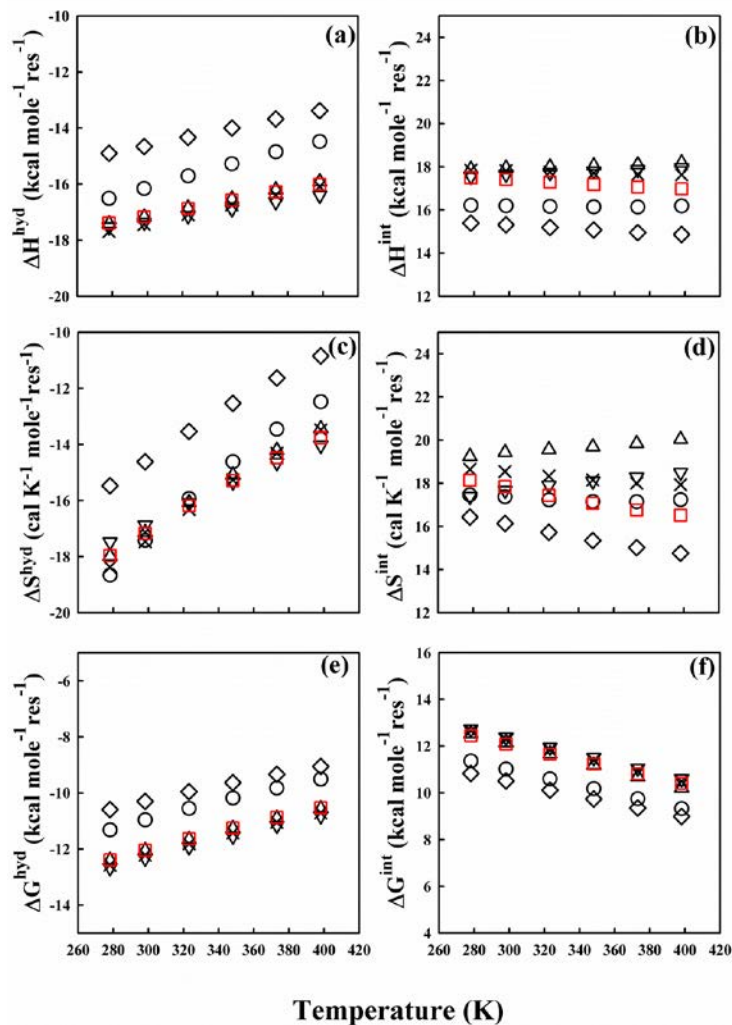


Figure S7. Delineation of the contributions of hydration and internal interactions to individual thermodynamic parameters. (a) shows the dependence of the hydration enthalpy per residue, $\Delta H^{\text{hyd}}/N_{\text{R}}$ on temperature. (b), (c) and (d) show the dependence of the enthalpy of internal interactions per residue, $\Delta H^{\text{int}}/N_{\text{R}}$, entropy of hydration per residue, $\Delta S^{\text{hyd}}/N_{\text{R}}$ and entropy of internal interactions per residue, $\Delta S^{\text{int}}/N_{\text{R}}$, respectively on temperature of moPrP (121-231) (□), barstar(○), bovine RNase A (▽), hen egg white lysozyme(×), barnase(△), and BPTI (◇).

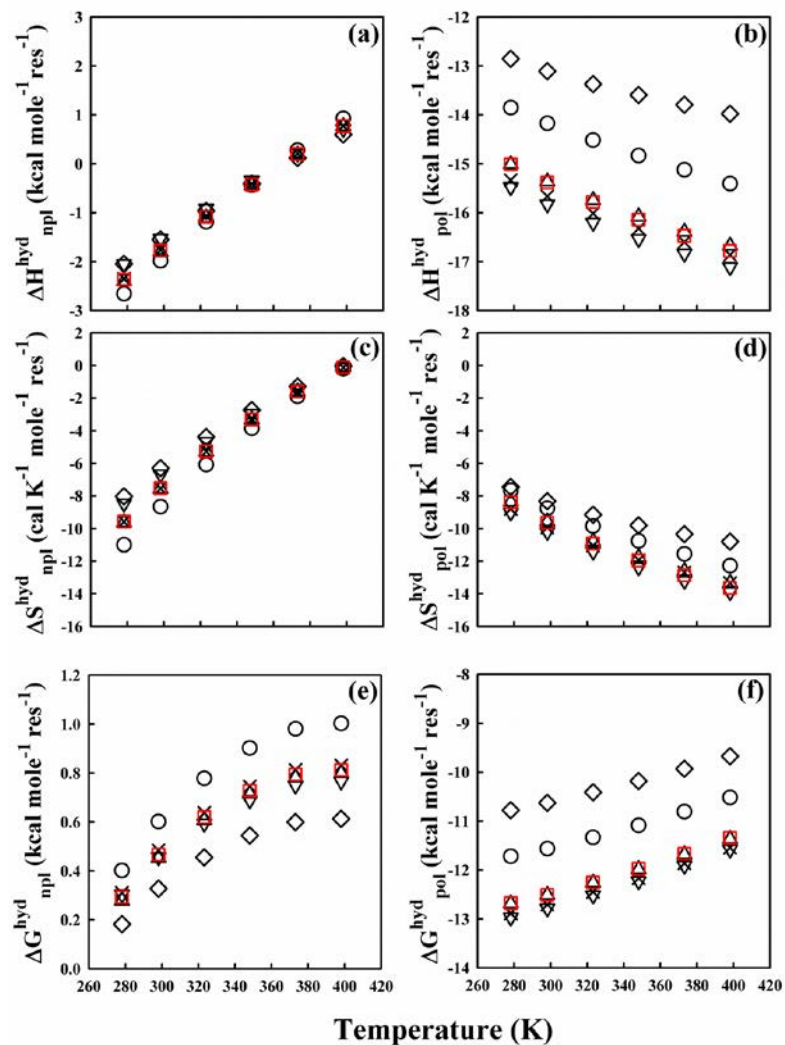


Figure S8: Temperature dependences of the hydration of polar and non-polar groups during unfolding. (a), (c) and (e) shows the dependences of the changes in the non-polar hydration enthalpy, $\Delta H_{\text{npl}}^{\text{hyd}}$, entropy $\Delta S_{\text{npl}}^{\text{hyd}}$, and Gibb's free energy, $\Delta G_{\text{npl}}^{\text{hyd}}$, respectively, on temperature, and (b), (d) and (f) show the dependences of the changes in polar hydration enthalpy, $\Delta H_{\text{pol}}^{\text{hyd}}$, entropy $\Delta S_{\text{pol}}^{\text{hyd}}$ and Gibb's free energy, $\Delta G_{\text{pol}}^{\text{hyd}}$, respectively, on temperature for moPrP (121-231) (\square), as well as for barstar (\circ), bovine RNase A (∇), hen egg white lysozyme (\times), barnase (\triangle) and BPTI (\diamond). The temperatures at which $\Delta H_{\text{npl}}^{\text{hyd}}$ and $\Delta S_{\text{npl}}^{\text{hyd}}$ equal zero are 366 K and 397 K for moPrP (121-231), 365 K and 398 K for barstar, 365 K and 398 K for bovine RNase A, 366 K and 397 K for hen egg white lysozyme, 367 K and 397 K for barnase, and 369 K and 396 K for BPTI, respectively.

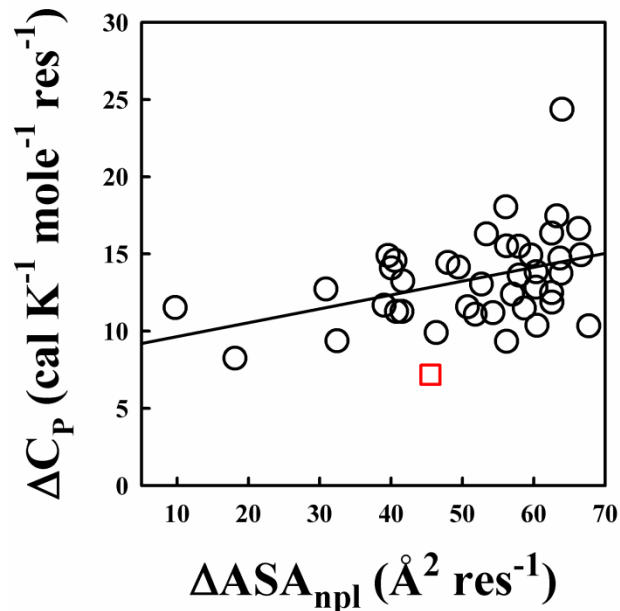


Figure S9. Comparison of the heat capacity change for the unfolding of moPrP (121-231) to that for the unfolding of other globular proteins. The change in heat capacity per residue upon unfolding is plotted against the average non-polar surface area, ΔASA_{npl} per residue that becomes exposed to water upon unfolding. Here, the ΔASA_{npl} for each protein is calculated considering the effect any disulphide(s) present, which reduces the accessible surface area of the unfolded protein (see Methods). Data for moPrP (121-231) (\square) is shown along with data for forty other proteins as listed in Robertson and Murphy (7). The solid line is a linear least-square fit. The ΔASA_{npl} for moPrP (121-231) has been corrected for the effect of residual structure in the unfolded state.

SUPPORTING REFERENCES

1. Liemann, S. and R. Glockshuber. 1999. Influence of amino acid substitutions related to inherited human prion diseases on the thermodynamic stability of the cellular prion protein. *Biochemistry*. 38:3258-3267.
2. Kholodenko, V. and E. Freire. 1999. A simple method to measure the absolute heat capacity of proteins. *Anal. Biochem.*270:336-338.
3. Squire, P. G. and M. E. Himmel. 1979. Hydrodynamics and Protein Hydration. *Arch. Biochem. Biophys.*196:165-177
4. Myers, J. K., C. N. Pace and J. M. Scholtz. 1995. Denaturant m values and heat capacity changes: Relation to changes in accessible surface areas of protein unfolding. *Prot. Sci.* 4: 2138-2148.
5. Makhatadze, G. I. and P. L. Privalov. 1993. Contribution of hydration to protein folding thermodynamics: I. The Enthalpy of Hydration. *J. Mol. Biol.* 232:639-659.
6. Privalov, P. L. and G. I. Makhatadze. 1993. Contribution of hydration to protein folding thermodynamics: II. The Entropy and Gibbs Energy of Hydration. *J. Mol. Biol.* 232:660-679.
7. Robertson, A. D. and K. P. Murphy. 1997. Protein structure and the energetics of protein stability. *Chem. Rev.* 97:1251-1268.
8. Agashe, V. R. and J. B. Udgaonkar. 1995. Thermodynamics of Denaturation of Barstar: Evidence for cold denaturation and evaluation of the interaction with guanidine hydrochloride. *Biochemistry*. 34:3286-3299.
9. Jain, S. and J. B. Udgaonkar. 2008. Evidence for stepwise formation of amyloid fibrils by the mouse prion protein. *J. Mol. Biol.* 382:1228-1241.
10. Vendrely, C., H. Valadie, L. Bednarova, L. Cardin, M. Padeloup, J. Cappadoro, J. Bednar, M. Rinaudo and M. Jamin. 2005. Assembly of the full-length recombinant mouse prion protein I. Formation of soluble oligomers. *Biochim. Biophys. Acta.* 1724:355-366.
11. Hornemann, S. and R. Glockshuber. 1996. Autonomous and reversible folding of a soluble amino-terminally truncated segment of the mouse prion protein. *J. Mol. Biol.* 261:614-619.
12. Privalov, P. L. and C. B. Anfinsen. 1979. Stability of proteins: small globular proteins. *Adv. Prot. Chem.* 33:167-241.
13. Schellman, J. A. 1978. Solvent denaturation. *Biopolymers.* 17:1305-1322.
14. Schellman, J. A. 1987. The Thermodynamic stability of proteins. *Annu. Rev. Biophys. Biophys. Chem.* 16:115-137.
15. Bolen, D. W., and M. M. Santoro. 1988. Unfolding free energy changes determined by the linear extrapolation method. 2. Incorporation of ΔG°_{N-U} values in a thermodynamic cycle. *Biochemistry*. 27:8069-8074
16. Chen, B. L. and J. A. Schellman. 1989. Low-temperature unfolding of a mutant of phage T4 lysozyme. 1. Equilibrium studies. *Biochemistry*. 28:685-691.
17. Lee, B. and F. M. Richards. 1971. The interpretation of protein structures: Estimation of static accessibility. *J. Mol. Biol.* 55:379-400.
18. Doig, A. J. and D. H. Williams. 1991. Is the Hydrophobic effect stabilizing or destabilizing in proteins? The contribution of disulphide bonds to protein stability. *J. Mol. Biol.* 217:389-398.